Colloquium: Reactive plasmas as a versatile nanofabrication tool

K. Ostrikov*

School of Physics, The University of Sydney, Sydney NSW 2006, Australia

(Published 22 June 2005)

The underlying physics of the application of low-temperature, low-pressure reactive plasmas in various nanoassembly processes is described. From the viewpoint of the "cause and effect" approach, this Colloquium focuses on the benefits and challenges of using plasma-based systems in nanofabrication of nanostructured silicon films, low-dimensional semiconducting quantum structures, ordered carbon nanotip arrays, highly crystalline TiO_2 coatings, and nanostructured hydroxyapatite bioceramics. Other examples and future prospects of plasma-aided nanofabrication are also discussed.

CONTENTS

I. INTRODUCTION

Fabrication of the various forms of nanostructured matter is at the heart of modern nanoscience (Roco *et al.*, 1999; Pitkethly, 2003). Various liquid, gaseous, solid, and colloidal systems (and their combinations), requiring different fabrication methods, have been successfully used as the precursor medium for myriad nanoscale assemblies. In this Colloquium, we discuss several unique features of low-temperature reactive plasma (also frequently called chemically active plasma) that make it an indispensable tool in a number of common nanoassembly processes.

The choice of any particular precursor medium and assembly method depends critically on the envisaged nanoscale object or assembly. Nonetheless, according to the commonsense "bricklayer's approach," most building processes, including nanoassembly, proceed in the following sequence: (i) selection and preparation of appropriate building units; (ii) preparation of the surface on which to deposit them; (iii) transport of the building units towards the assembly, and (iv) appropriate stacking of building units to create the assembly. Whether the assembly is a conventional brick wall or an exotic nanostructure, it commonly requires a sequence of appropriate manipulations of the building units. Let us consider what this means in the context of plasma-assisted nanofabrication. Our focus here will be on the plasma-assisted generation of the building units, their deposition onto the surface, and their stacking into the desired nanoassembly patterns.

The generation and assembly of building units into nanofilms and nanostructures are processes that tend to be specific to the medium and the desired structure. However, extensive ongoing research has been focused on finding common physical features of the growth →transport→deposition→assembly chain in various nanofabrication processes.

This Colloquium comprises three main sections, plus a Conclusion and Outlook section. In Sec. II, the potential interest of reactive plasma in nanofabrication is considered, based on its ability to generate a broad range of sizes and species. Reactive plasma environments are also able to enhance chemical vapor deposition and help to maintain an even substrate temperature. In Sec. III, in comparison with thermal chemical vapor deposition systems, we consider the features of reactive plasmas that make them particularly attractive for nanoscale applications. In particular, the ease with which building units can be manipulated within the plasma and deposited compares favorably with thermal methods in which manipulation is inefficient. In Sec. IV, examples of specific nanofabrication processes are critically examined to illustrate the benefits and challenges of using plasma-based systems in fabrication of many nanostructures—semiconducting nanostructured films and low-dimensional quantum structures, ordered arrays of carbon nanotips, cluster-assembled crystalline TiO_2 films, and nanostructured hydroxyapatite biocompatible coatings. The concluding section is focused on the conceptual framework and future challenges for reactive-plasma-assisted nanofabrication.

II. GENERAL CONSIDERATIONS

The first "nanobuilding" step is to generate the required building units with the desired chemical organization, size, and morphology. They must also be created

*Also at: Plasma Sources and Applications Center, NIE, Nanyang Technological University, 637616 Singapore. Electronic address: K.Ostrikov@physics.usyd.edu.au

in certain energetic, charging, and bonding states. The use of reactive plasma makes it possible to generate the entire range of species, from atoms, molecules, ions, and radicals to macromolecules, nanosized clusters, nucleates, particulates, and complex aggregates and agglomerates. Plasma-assisted nanoassembly techniques include gas-phase ionization, dissociation, and polymerization processes. At this point it is reasonable to pose the question: how does one differentiate between reactive and ordinary plasma? Reactive plasmas are usually composed of multiple reactive species that continuously transform into each other and that also generate new species as a result of numerous chemical reactions in the ionized gas phase (Fridman and Kennedy, 2004). Consequently, mutual transformations and chemical reactivity of the species is what makes these plasmas different from conventional multicomponent plasmas. We recall that chemical reactivity of the species is often associated with dangling (activated, or available for bonding) chemical bonds, another feature that is useful in nanoassembly.

The generation of building units in reactive plasmas is a very complex process and is mediated by a large number of elementary reactions in the ionized gas phase. For example, units of lower atomic mass (e.g., atoms, molecules, radicals, and ions) are usually generated through gas-phase electron-impact or heavy-particle collisional ionization or dissociation of the feedstock gas. Alternatively, they can be released from solid surfaces exposed to plasmas as a result of physical sputtering or chemical etching processes. Yet another possibility is that the building units can be generated on the deposition surface as a result of the breakup of larger building units into nanofragments, atoms, and/or radicals.

Larger building units can be generated as a result of complex polymerization or clustering processes in the gas phase, or via the release of various nanofragments from the solid surfaces. Gas-phase polymerization is usually triggered by certain reactive precursor species (e.g., anion SiH_3^- in silane-based plasmas) and proceeds, through a chain of polymerization reactions, to macromolecules (which can be either neutral or charged) and critical clusters, which are large enough to trigger the nucleation process (Perrin and Hollenstein, 1999; Hollenstein, 2000). Having reached a critical number density, solid surface-released species can form larger clusters, which become nucleation precursors. The sizes of critical clusters depend on specific plasma parameters and are typically less than a few nanometers.

Generally speaking, building unit generation can be managed through adjustment of the rates of the major elementary reactions in the plasma, which can be achieved by varying the discharge control parameters. The simplest way is to adopt a trial and error approach and achieve the required composition and other properties of the building units through a large number of trial experiments. One could also attempt a fully self-consistent and systematic approach to this problem, which would require knowledge of all the reactive species and chemical reactions involved in the generation of the building units (very often in the hundreds). A third method would be to start with the structure desired, then consider the main precursors and other conditions for generation of appropriate building units, which could be called the "cause and effect" approach. Using any one of the three aforementioned approaches, one can optimize the process parameters for the gas-phase generation of the desired building units.

The next two steps, (ii) and (iii), can be carried out either sequentially or simultaneously. In either case, the deposition surface must be suitably prepared before the building units can land on it. Again, the requirements for surface preparation are process specific. For example, if a nanoassembly requires certain reactive radicals with a single dangling bond, an adequate number of compatible dangling bonds should be available at the required surface sites, where the nanostructure is being assembled (Poole and Owens, 2003). As another example, deposition of gas-phase nucleated nanocrystals or nanoparticles would require a suitable (e.g., amorphous) matrix, or otherwise prepared surface with the required adhesive properties to secure the building units—either by embedding them within or attaching them to the surface. Nanoassemblies often require specific (e.g., thermal) activation of catalyst layers. For example, growth of carbon nanotubes usually requires thermally activated fragmentation of thin (a few to a few tens of nm) Ni/Fe/Co catalyst layers into nanosized particles forming a wetting contact with the substrate (e.g., silicon or glass) (Iijima, 1991; Bethune *et al.*, 1993). Reactive plasma environments make possible many kinds of surface preparation. The available options range from surface heating, activation, and physical sputtering by intense ion fluxes accelerated in the plasma sheath to plasma-enhanced chemical vapor deposition (PECVD) of passivating or adhesive, nanolayers on the deposition surface, and selective and highly anisotropic reactive chemical etching of the nanostructure growth surface. It is relevant to mention that some of the above processes affect the nanostructures being grown. For example, reactive chemical etching is an important reshaping (e.g., sharpening) factor in the growth of various carbon nanostructures. This will be discussed in greater detail in Secs. III and IV.

The next step is to transport the building units to the nanoassembly being targeted. In this regard, one has to keep in mind several basic possibilities and challenges. First, it is possible to transport the building units anywhere onto the surface and then rely on their surface migration from the deposition point to the nanoassembly. Another possibility is to transport the building units directly to the nanoassembly being grown and arrange their stacking directly from the gas phase, without any need for surface migration. As will be discussed below, the importance of the second transport channel becomes greater in reactive plasmas due to intense ion fluxes that originate in the plasma sheath and converge towards sharper tips of some nanostructures, such as carbon nanoneedles or nanotips, discussed in Sec. IV.B. Second, it is crucial that the building units be transported to a

suitably prepared surface area in such a way as to preserve their integrity, i.e., without breaking apart into smaller fragments. In reactive plasmas, this process can be controlled by manipulation of the fluxes of the plasma species and the building unit driving forces (e.g., electrostatic and ion drag forces) in the near-substrate areas (Sec. III.C). Another practically important option is to implement a time-resolved separation of building-unit growth and transport stages by transporting them to the surface in the discharge afterglow (after switching the plasma off).

The last step is to ensure that the building units are appropriately stacked into the required nanoassembly pattern. Once a building unit has reached the nanoassembly, further integration becomes ultimately controlled by the self-assembly (or self-organization) processes on the nanoscale (Poole and Owens, 2003; Stangl *et al.*, 2004) and at this stage is less directly affected by the reactive plasma. Nevertheless, the reactive plasma medium can provide important ambient conditions for the nanoscale assembly to proceed. For example, if the discharge is run continuously, intense fluxes of ions and neutrals dynamically maintain the equilibrium substrate temperature, which is the key control factor at this stage, often making external temperature control superfluous. It is imperative that, depending on the surface activation performed during the second stage, the development of nanostructured films or nanoassemblies be able to proceed either through the island or layer-by-layer growth scenarios (Shuchukin *et al.*, 2003). The latter mechanism usually requires a greater precision in homogeneous activation of surface dangling bonds over large areas.

In the following sections, we shall consider how to implement the aforementioned four-step nanofabrication process by capitalizing on the unique properties of reactive plasmas. We shall highlight the unique ability of reactive plasmas to generate the desired building units (encompassing the entire range of the species, from atoms and molecules to nanosized clusters, particulates, and agglomerates) through gas-phase ionization/dissociation and polymerization processes in the PECVD of selected nanoassembles. We shall also compare the underlying physical phenomena in reactive plasmas with those of some other common nanofabrication methods and discuss the advantages and benefits of using the plasma-assisted techniques.

For example, carbon nanotubes can be synthesized by either thermal or plasma-assisted chemical vapor deposition in carbon-bearing precursors such as methane, acetylene, etc., mixed with other inert or reactive gases (Iijima, 1991; Dresselhaus *et al.*, 1996). Thermal chemical vapor deposition usually requires very high gas temperatures (and also quite often high pressures) to decompose the feedstock gas, which adversely affects the suitability of this process for technologies that require low temperatures such as metal interconnects in semiconductor micromanufacturing. By using a reactive plasma, one can achieve a substantial precursor dissociation into numerous ionic and radical species. In this case, one can noticeably lower the process temperatures and achieve much higher deposition rates. However, it is generally believed that plasma-assisted chemical vapor deposition is not suitable for the fabrication of single-walled carbon nanotubes, which are easily synthesized by thermal chemical vapor deposition methods (Meyyappan *et al.*, 2003).

In this Colloquium, we focus on typical reactive-plasma-based PECVD systems and point out the features of such systems that make them particularly attractive for numerous nanoscale applications. In particular, we aim to clarify the following (and some other) issues:

- When and why is it more beneficial to use either thermal chemical vapor deposition or PECVD? In which cases should one use the plasma and in which cases not?
- How does one develop the process to fabricate the desired nanofilms?
- What is the actual role of the plasma in the PECVD of nanofilms and nanostructures?
- How do plasma sheaths, precursor dissociation, and plasma polymerization affect the nanoassemblies being targeted?
- How does one transport plasma-grown building units to the deposition surface and stack them into the required nanoassembly pattern?

By comparing the underlying physics with common thermal chemical vapor deposition systems, we highlight the most striking features, benefits, and challenges of using PECVD systems in several typical examples of nanofabrication, including but not limited to ordered carbon nanotips, nanostructured silicon films, semiconductor quantum dot arrays, and nanostructured calcium phosphate biocompatible films. Special attention will be paid to the identification and control of the main building units.

III. SPECIFIC FEATURES OF REACTIVE PLASMAS

In this section, we identify and discuss the key features of reactive plasmas used in plasma-enhanced chemical vapor deposition (PECVD) of various nanostructured films and nanostructures. By following the same sequence of nanofabrication steps and other important considerations, we also compare the performance of the PECVD systems with the commonly used thermal chemical vapor deposition (CVD) systems.

A. Basic features

In PECVD systems, thin films are usually deposited on a solid surface as a result of plasma-surface interactions in the gas-solid environment, as schematically shown in Fig. 1. The entire near-surface area can be separated into three distinctive regions, namely, plasma bulk, plasma sheath, and solid substrate, with the outer layer (growth surface) facing the plasma. Each of the

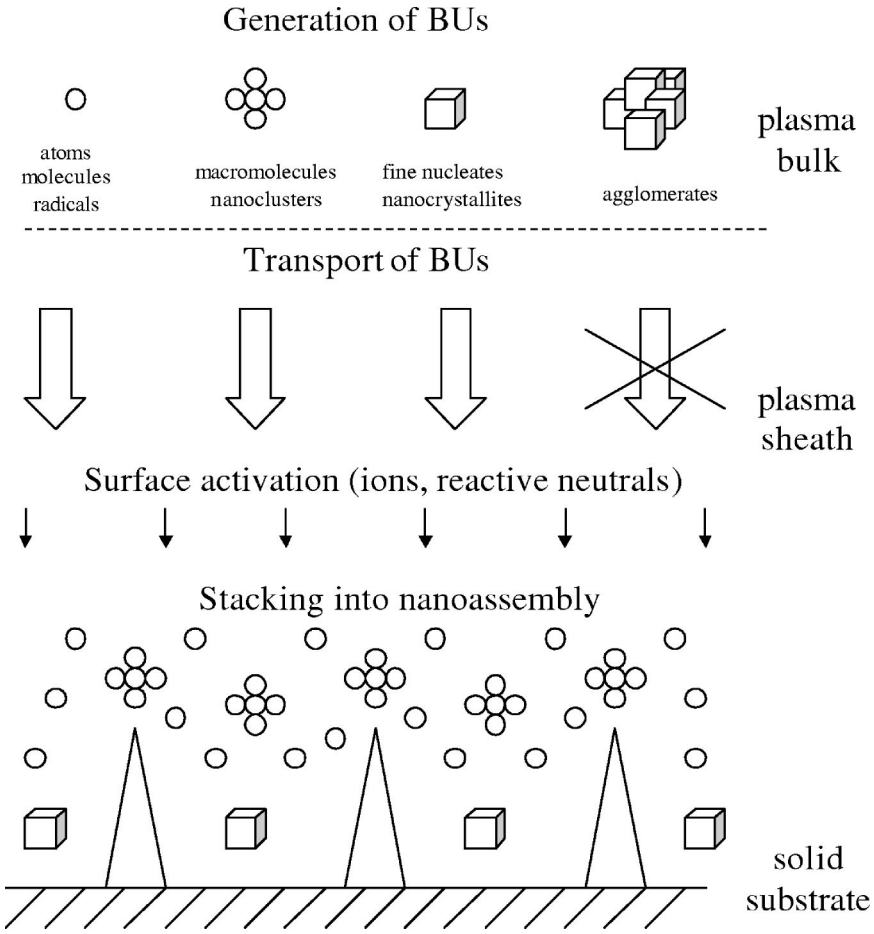

FIG. 1. Schematics of the reactive-plasma-based nanofabrication environment. BU =building unit.

above regions plays its specific role in the four-step nanofabrication process of interest.

As a point of reference, we recall that common thermal CVD-based nanofabrication processes capitalize on the interactions of a hot reactive gas with suitably preprocessed deposition substrates, which can be additionally heated externally during CVD. In most cases, the gas feedstock remains neutral in the chamber bulk, as its thermal ionization would require very high temperatures. For example, thermal dissociation of methane, commonly used in the fabrication of various carbon nanostructures, is negligible even at gas temperatures of $\sim 900\,^{\circ}\mathrm{C}$ (Franklin and Dai, 2002). However, ionized species can be created on heated surfaces as a result of Saha-Langmuir ionization (Fridman and Kennedy, 2004). If a reactant gas pressure in a CVD reactor exceeds a certain threshold, typically of the order of 100 mTorr, gas-phase clustering processes often result in the appearance of neutral nanosized clusters, which can become ionized upon landing on the surface (Hwang and Yoon, 1994). On the other hand, charged clusters can be generated as a result of nucleation induced by ions released from the surface. Thus thermal CVD systems usually feature a limited number of building units, such as thermally activated atoms or molecules and nanoclusters. However, in many cases only nanoclusters stand a chance to be the dominant building units of various nanofilms and nanostructures, as atomic and molecular CVD features extremely low deposition rates. Moreover, smaller and charged nanoclusters are more favorable for epitaxial recrystallization upon landing on the surface, whereas larger and neutral clusters usually coagulate to form cauliflower and porous skeletal structures (Hwang and Kim, 2004).

On the other hand, in PECVD the gas phase is a two-component system and comprises the neutral and ionized gas (plasma) components. In a weakly ionized plasma the relative population of the ionized component $\Sigma_j n_i^j / \Sigma_k N_n^k$ is low, where n_i^j and N_n^k are the number densities of jth ionic and kth neutral species, respectively. Thus the presence of the neutral component makes PECVD similar to most of the commonly used CVD systems. However, the presence of the additional ionized phase makes a remarkable difference at all four stages of the nanofabrication process.

The most striking difference is the presence of the *plasma sheath*, which is a non-neutral layer of space charge separating the plasma bulk and the solid substrate. Because of the much higher mobility of electrons, the surface is always charged negatively with respect to the plasma bulk (Lieberman and Lichtenberg, 1994). The resulting potential distribution sustains intense positive-ion fluxes onto the surface and impedes the fluxes of negatively charged species. The plasma bulk acts as an efficient ionizer of the neutral gas, where a broad spectrum of positively and negatively charged

ionic species is generated. As a result of numerous electron-impact and heavy-particle collisions, neutral molecules are dissociated into reactive radical fragments. Meanwhile, large populations of negative ions in common reactive plasmas (e.g., $SiH_4, C_4F_8, SF_6, O_2, Cl_2$, etc.) are favorable for ion-induced polymerization and clustering, giving rise to larger macromolecules and nanoclusters (Perrin and Hollenstein, 1999; Hollenstein, 2000; Fridman and Kennedy, 2004). The negative surface potential contributes to longer residence and confinement of negative-ion precursors and negatively charged clusters and macromolecules in the transition area (commonly called the *presheath*) between the plasma bulk and the sheath, which is impossible in a thermal CVD. In a sense, the plasma sheath protects the deposition surface against the fallout of negatively charged ions, clusters, or nanoparticles (Vladimirov and Ostrikov, 2004). Surprisingly, this is the case even when a large positive bias is applied to the substrate, as the potential distribution in the plasma is rearranged to maintain lower surface potentials with respect to the plasma bulk (Lieberman and Lichtenberg, 1994). Under certain conditions, primary macromolecules and nanoclusters can nucleate to form nanosized amorphous or crystalline particles. Thus, in PECVD, the films can be deposited by a larger variety of building units than in thermal CVD processes. It is important to note that, in contrast to CVD processes, the ionization/dissociation of the neutral-gas feedstock and larger building units are usually less likely on the deposition surface than in the gas phase. Before we proceed to consideration of specific features of plasma-based nanofabrication owing to the presence of the plasma sheath, let us discuss how to choose and generate the desired building units.

B. Generation of building units

As we have mentioned above, reactive plasmas can generate the entire range of potential building units in atomic, molecular, cluster, and other forms. How does one choose which kind of units to generate and which specific control strategies, suitable for reactive plasmas, to use in fabricating the desired nanoassembly? Clearly, this question has no single answer, with the number of possible solutions exceeding the number of nanoassemblies ever fabricated by plasma-based methods. However, one can narrow the possibilities by taking the "cause and effect" approach to the sequence: precursor →building unit(s)→nanostructure (with a feedback/optimization loop, as shown in Fig. 2), supported by existing knowledge from other areas of nanoscience. Without trying to provide exhaustive recipes for the appropriate choice of building units, we start with the structural considerations of the nanostructures being created and work backwards, taking into account the established theories of growth kinetics on the nanoscale (Poole and Owens, 2003; Shchukin *et al.*, 2003; Stangl *et al.*, 2004).

For example, in the assembly of single-walled or multiwalled carbon nanotubes, it is widely accepted that one

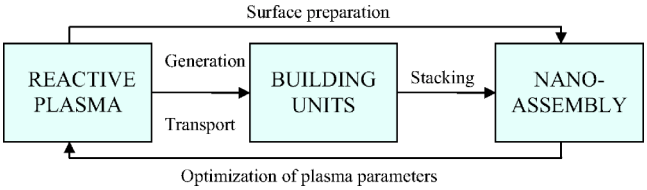

FIG. 2. (Color in online edition) Simplified concept map of the reactive-plasma-based cause and effect nanofabrication approach.

should use reactive dimers C_2 (Dresselhaus *et al.*, 1996). In particular, the chemical structure and reactivity (usually characterized by the availability of dangling bonds and energy barriers for specific interactions) of the C_2 molecule are ideal for its insertion in graphite hexagonal lattice patterns that build up the carbon nanotube walls (Shchukin *et al.*, 2003). On the other hand, the carbon dimer also plays a prominent role in the plasma-assisted synthesis of ultrananocrystalline diamond (Gruen, 2001). It is important that the C_2 is a highly energetic molecule that can be inserted directly into carbon-carbon and carbon-hydrogen bonds, often without any intermediaries, such as the reactive hydrogen atoms that are frequently used for the activation of dangling bonds on hydrocarbon-based surfaces. This mechanism is responsible for the self-assembly of dimer rows of the reconstructed surfaces of ultrananocrystalline diamond (Gruen, 2001). Here, the carbon dimer represents a typical molecular building unit.

Nanosized clusters, macromolecules, and nanofragments (hereafter collectively termed nanoclusters) form an intermediate group of building units (Fig. 1), with sizes ranging from less than one to a few nanometers. The building units of this category usually participate in the nanofabrication processes concurrently with other units and often appear as a product of atomic/molecular clustering or complex chains of polymerization reactions in the gas phase (Yasuda, 1985; Perrin and Hollenstein, 1999). According to charged-cluster theory, negatively charged carbon clusters with sizes not exceeding a few nanometers and containing a few hundred carbon atoms are the ideal building units for epitaxial growth of single-crystalline diamond, whereas larger ($>$1000 atoms and up to $\sim$10 nm) and positively charged hydrogenated carbon clusters are required for the synthesis of amorphous or crystalline graphite (Hwang *et al.*, 1996; Hwang, 1999). These conclusions of charged-cluster theory have been confirmed by measurements of charged-nanocluster mass and size distributions in hot filament CVD reactors and hydrocarbon-oxygen flames (Gerhardt and Homann, 1990; Jeon *et al.*, 2000). Likewise, the polarization properties of small silicon nanoclusters make them ideal building units capable of selectively attaching to elongated silicon nanostructures such as silicon nanowires, carbon nanoneedles, and some others (Hwang *et al.*, 2000; Xu, Ostrikov, *et al.*, 2005).

One of the most recent examples of how a specific arrangement of building units can result in an exotic nanostructured organization of matter is the fifth known

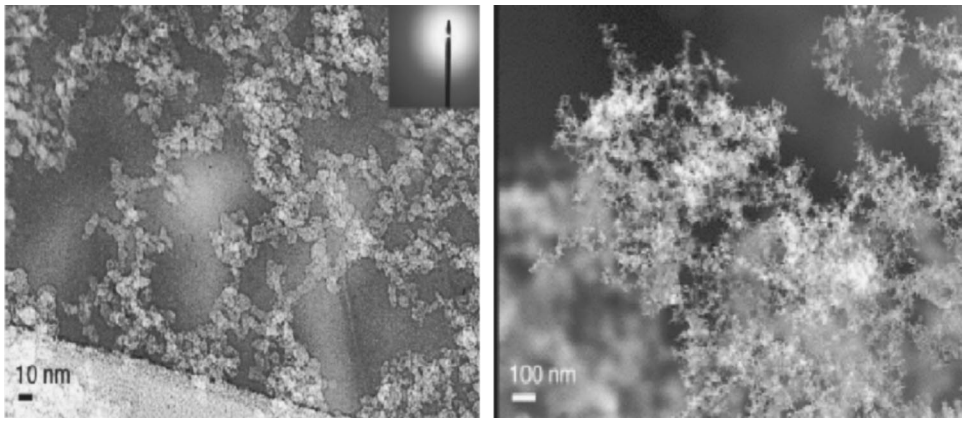

FIG. 3. Transmission electron micrograph (left image), and scanning electron micrograph (right image) of carbon nanofoam, showing its weblike structure. From Rode *et al.*, 2004.

(in addition to graphite, diamond, fullerenes, and carbon nanotubes) allotrope of carbon, known as *carbon nanofoam*, shown in Fig. 3 (Rode *et al.*, 2004). Carbon nanofoam, which has both ferromagnetic and semiconducting properties, is made of a web of randomly interconnected carbon-atom clusters, with an average diameter of 6–9 nanometers. These can be seen in the transmission electron microscopy (TEM) image in Fig. 3. The unexpected magnetic properties of this new material can be attributed to the unusual organization of carbon atoms in the clusters: carbon atoms in the foam form heptagonal structures with an unpaired (and thus not involved in chemical bonding) electron, which has a magnetic moment that may lead to magnetism. Note that only pure carbon atoms are involved in the formation of the carbon nanoclusters that serve as building units of carbon nanofoam (Rode *et al.*, 2004).

On the other hand, higher silanes (macromolecules) and hydrogenated silicon clusters play a pivotal role in the plasma-assisted deposition of nanostructured amorphous films for solar-cell applications. The gas-phase concentration of higher silanes in the silane-based PECVD of *a*-Si films controls the film deposition rate and directly correlates with the microstructure and performance of the solar-cell elements (Tanda *et al.*, 2003). The number of small (less than a few nm in size) hydrogenated silicon clusters in silane discharges directly correlates with the microstructure parameter, which is one of the indicators of the device quality of *a*-Si:H films (Shiratani *et al.*, 2003). One of the advantages of the use of larger than atomic/molecular building units is the prospect of significantly enhancing the film deposition rates. For example, high rates of deposition of nanostructured carbon films can be achieved by the supersonic cluster beam deposition technique (Magnano *et al.*, 2003). However, one should also keep in mind that excessive concentrations of nanoclusters can compromise some film performance specifications, which are critical in industrial applications.

Larger clusters, nanocrystallites, and complex aggregates (hereafter collectively called nanoparticles) can be regarded as the third distinctive group of plasma-generated building units. These can be intentionally grown in the gas phase and incorporated into the growing film. For example, silicon films grown with a significant contribution of nanoparticles coming from the plasma have been found to exhibit improved transport and stability properties, as well as a wider optical band gap than nanoparticle-free *a*-Si:H. Structural incorporation of the plasma-grown nanoparticles (usually a few nm in size) has made it possible to synthesize polymorphous silicon (*pm*-Si:H) films, a unique form of nanostructured matter featuring an ordered amorphous matrix with nanocrystalline inclusions (Viera *et al.*, 2002). It is noteworthy that recent results show that performance of PIN solar cells (*p*-type semiconductor/insulator/*n*-type semiconductor) can be significantly improved through nanocrystalline (usually 1–2 nm) inclusions deposited with high rates in silane-based PECVD (Poissant *et al.*, 2003; Fontcuberta i Morral *et al.*, 2004; Suendo *et al.*, 2004). Further disussion of this effect can be found in Sec. IV.A.

It is interesting to note that charged clusters appear in the gas phase of reactive plasmas at much lower pressures than are typically required in thermal CVD systems. For example, in the CVD synthesis of diamond, gas-phase generation of charged clusters requires supersaturated reactive gas feedstock and hence higher working pressures, typically in excess of ~100 mTorr (Hwang and Yoon, 1994). By contrast numerous reports suggest efficient polymerization and clustering processes in reactive plasmas at working gas pressures as low as a few mTorr (Perrin and Hollenstein, 1999; Hollenstein, 2000).

Furthermore, single-crystalline nanoparticles in the gas phase of reactive plasmas are promising as building units in the fabrication of quantum communication, molecular electronics, data storage, and light-emitting devices (Bapat *et al.*, 2003). Some elements of these devices, such as field-emitting arrays of vertically aligned single-crystalline carbon nanotips/nanoneedles, ordered $Al_xIn_{1-x}N$, $Si_{1-x}C_xN$ quantum dot structures, and silicon nanowires, can also be fabricated in reactive plasmas by using smaller atomic/radical and nanocluster units (Xu, Ostrikov, *et al.*, 2005).

Electronic and other properties of nanocluster and nanoparticle assembled bulk materials show clear dependence on the size of the building units. Indeed, quantum size effects can strongly affect the arrangement of crystal lattices and electronic spectra of building units in the 1–10-nm size range. For example, gold nanoparticles change color from reddish-blue to orange and even become colorless when their size decreases from 30 to 1 nm (Mulvaney, 2001), which is in remarkable contrast to the yellowish color of conventional bulk gold. Notably, nanoparticles feature quite different (strained) chemical structures from those of bulk materials, a feature that has numerous implications for nanocomposites and nanoelectronic systems (Gilbert *et al.*, 2004).

We note that complex aggregates (generated as a result of agglomeration of smaller building units) are usually considered as unwelcome side products and should be avoided in reactive-plasma-assisted nanofabrication (Fig. 1). However, freestanding nanoparticles can be confined, coated, functionalized, etc. For example, decomposition of the reactive precursor ATI $[Al(i\text{-}OC_3H_7)_3]$ in Ar-based rf plasmas has been used to deposit thin alumina films on barium magnesium aluminate fine particles used as high-brightness phosphors in tricolor fluorescent lamps (Kersten *et al.*, 2003).

C. Sheath-related features

The plasma sheath plays a significant role during the surface activation and building unit transport stages. Indeed, the electric field of the uncompensated space charge drives positively charged species towards the solid surface and slows down the motion of negatively charged species. This polarity of the near-substrate electric field strongly enhances the surface fluxes of positively charged building units, which are otherwise quite small in thermal CVD systems. Meanwhile, negatively charged species can be suspended by the sheath potentials and, residing in the discharge longer than neutral and positively charged species, are able to efficiently mediate plasma polymerization processes (Yasuda, 1985; Fridman and Kennedy, 2004). Depending on the size of the building units and prevailing experimental conditions, other plasma forces can come into play. The motion of building units in the subnanometer range (i.e., atoms, molecules, radicals), can be impeded as a result of collisions with other (usually mostly neutral in weakly ionized plasmas) species in the sheath. The resulting frictional force can divert the building units from the deposition surface, leading to chaotic and oblique deposition after a number of collisions. This effect is important for collisional sheaths, when $\lambda_s > \lambda_{mfp}$, where λ_s and λ_{mfp} are the sheath width and mean free path of positively charged building units in collisions with other plasma species. On the other hand, in collisionless sheaths ($\lambda_s \ll \lambda_{mfp}$), the positively charged building units move smoothly along the electric-field lines directed normally to the surface. The latter case is most common in low-pressure PECVD reactors used for plasma-assisted nanofabrication. In particular, it is commonly accepted that the normal direction of the sheath electric field is a reason for vertical alignment (generally speaking, normal to the substrate, depending on the sample orientation) of carbon nanotubes (Bower *et al.*, 2000; Chhowalla *et al.*, 2001).

However, the effect of the degree of collisionality of the plasma sheath on the properties of reactive-plasma-grown nanostructures still requires further study. An important implication is that neutral building units (e.g., the carbon dimer C_2), unaffected by the sheath electric field, can be transported through the collisionless sheath without any significant change of their energetic state acquired in the plasma bulk as a result of intense collisions with other neutral and ionized species. Indeed, the electron-depleted plasma sheaths effectively exclude electrons from electron-impact excitation of the neutral building units, whereas heavy-particle collisions become inefficient when $\lambda_s \ll \lambda_{mfp}$. Thus the reactivity (determined by the energetic state) of the neutral building units (essential for their insertion into nanoassemblies or reconstructed surfaces of bulk materials) can be controlled by adjusting the rates of collisions in the plasma bulk and is not expected to change within the collisionless plasma sheath.

Larger (>1 nm) building units are subject to some other forces, such as ion and neutral drag forces, thermophoretic forces, and gravity (Vladimirov and Ostrikov, 2004). The above forces scale differently with particle size, which opens up the possibility of manipulating building units by adjusting the force balance on them. Gravity is usually weak for building units suitable for nanofabrication purposes. In most cases, negatively charged units are repelled by the negative substrate potentials. However, under certain conditions they can overcome repulsive potential barriers and be deposited on the surface. Manipulation of nanoparticles in reactive plasmas will be discussed further in Secs. IV.A and IV.B.

More importantly, the plasma sheath potentials control the fluxes and energies of the charged building units impinging on the surface. For better-quality films and perfect nanostructures, it is generally required that the building units land on the surface without disintegration into smaller fragments (more common for larger units, >1 nm) and/or without damaging the activated surface sites prepared to host them (more common for sub-nm units). For example, nanocluster deposition techniques are extremely sensitive to the landing energy and orientation of the clusters (Frantz and Nordlund, 2003; Hwang and Kim, 2004). If a cluster is small enough (e.g., a few nm), the substrate surface hot enough (600–1000 °C), the lattice mismatch between the cluster and the substrate small enough, and the cluster incident normal to the surface with a low energy (fractions of eV to a few eV), then epitaxial recrystallization of the cluster atoms in the substrate lattice is likely, with the initial stage shown in Fig. 4 (left). In this case the lattice of the cluster can ideally fit into the substrate lattice and rearrange through vacancy migration along the cluster-substrate interface (Frantz and Nordlund, 2003). However, clusters with larger size, higher energy, and oblique

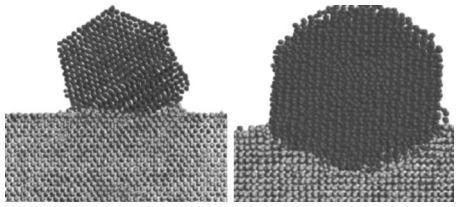

FIG. 4. Initial stages of epitaxial recrystallization (left image) and burrowing (right image) of a 4876-atom Co nanocluster deposited on a Cu(100) surface. The burrowing is accompanied by formation of well-resolved grain boundaries. From Frantz and Nordlund, 2003.

incidence have less chance for epitaxial recrystallization and usually only partially burrow into the substrate, forming distinct grain boundaries within the substrate material and islandlike structures on the surface (Fig. 4, right). In this case, the rearrangement proceeds through disordered motions of atoms along the cluster-substrate interface (Frantz and Nordlund, 2003). Furthermore, very small clusters (1–2 nm), with no fixed crystalline orientation and featuring a lower melting point compared to bulk materials are able to adopt the crystal structure of the substrate or film already deposited. Hence perfectly crystalline films can be grown by epitaxial recrystallization of small nanoclusters (Hwang and Kim, 2004). Larger clusters tend to retain their ordered structure upon deposition, resulting in nanostructured films with well-defined grain boundaries. Interestingly, the sheath electric field also controls alignment of dipole building units in the vicinity of the deposition surface. Thus the insertion of radical and molecular building units with dipole moments into nanoassemblies is quite different in plasma-aided processes.

The electric field in the plasma sheath is an additional powerful tool to control the energy and incidence angle of the building units. However, large sheath potentials can be detrimental to the integrity of charged-nanocluster building units. For example, nitrogen clusters break up upon landing on graphite surfaces if the potential difference between the surface and the plasma bulk is of the order of 25 V (Roca i Cabarrocas *et al.*, 2004). In this case, most of the deposition material carried by the clusters is washed back to the gas phase, with a small fraction embedded as defects in the substrate crystalline structure. Thus, in nanofabrication processes using charged nanoclusters, one should adjust the sheath width and potential distribution to avoid structural damage to the building units. For example, if $\tau_b \gg \tau_i$, where τ_b is the duration of the applied bias pulse and τ_i is the ion motion time scale, the sheath width,

$$\lambda_s = (\sqrt{2}/3)\lambda_D(2eV_0/T_e)^{3/4}, \tag{1}$$

and the potential profiles $\phi(x)$ near the substrate (located at $x=-\lambda_s$),

$$\phi(x) = -\left(\frac{3}{2}\right)^{4/3}\left(\frac{J_0}{\epsilon_0}\right)^{2/3}\left(\frac{2e}{m_i}\right)^{-1/3}x^{4/3}, \tag{2}$$

can be related to the plasma parameters and adjusted to ensure the required energy and flux of the building units (Lieberman and Lichtenberg, 1994). Here, λ_D is the Debye length, V_0 is the bias potential, T_e is the electron temperature, m_i is the ion mass, and $J_0 = en_{iS}V_B$ is the ion current entering the sheath, where n_{iS} and $V_B = (T_e/m_i)^{1/2}$ (Bohm velocity) are the ion number density and velocity at the sheath edge, respectively. In deriving Eqs. (1) and (2), it was assumed that $eV_0 \gg T_e$ and it was noted that the potential near the solid surface was lower than in the plasma bulk.

It is important to keep in mind that plasma sheath potentials also sustain intense fluxes of energetic ions onto the substrates. The ion fluxes make a major contribution to physical sputtering and reactive chemical etching of deposition surfaces, as well as activation and passivation of surface bonds. Likewise, they directly heat the deposition substrates and adjacent gas through intense ion-surface and ion-neutral collisions. In some cases, direct heating of deposition substrates by ion fluxes and hot gas in the reactor makes any external substrate heating unnecessary. For example, some of the ordered carbon nanostructures discussed in Sec. IV.B have been grown under no-external-heating conditions. Meanwhile, nanoparticles confined in near-substrate areas of reactive plasmas can be "annealed" *in situ* by hot ambient gas and ion fluxes, which can result in sintering and eventual spheroidization of the building units by the plasma-enhanced surface self-diffusion of atoms (Perrin and Hollenstein, 1999). In this way, individual nanoparticles that were initially unsuitable for device or film integration can be etched and post-processed (Stoffels *et al.*, 1999) to become viable building units for nanofabrication.

An interesting example of the role of the plasma in the preparation of solid surfaces is the surface reaction kinetics of SiH_3 and CH_3 building units in the reactive-plasma-assisted deposition of hydrogenated amorphous silicon and carbon films (Perrin *et al.*, 1998). A difference in chemical structure is the main reason for the remarkably different surface interactions of SiH_3 and CH_3 radicals with the growing surfaces. The SiH_3 molecule has a pyramidal structure and a permanent dipole moment, whereas CH_3 is planar. In a sense, the dipole moment is a measure of the reactivity of SiH_3 radicals, capable of using the dipole interaction to abstract hydrogen from the growing *a*-Si:H surface and thus activate a dangling bond on the surface, as shown in Fig. 5 (left). The vacated dangling bond can be instantly occupied by another chemisorbed SiH_3 radical. In this case, the film growth is supported by a vacancy migration along the plasma-silicon interface and is quite similar to that involved in epitaxial recrystallization of small nanoclusters discussed above. On the other hand, planar methyl radicals do not have any dipole moment and rely heavily on creation of dangling bonds either by ion bombardment or by reactive hydrogen atoms generated in the plasma

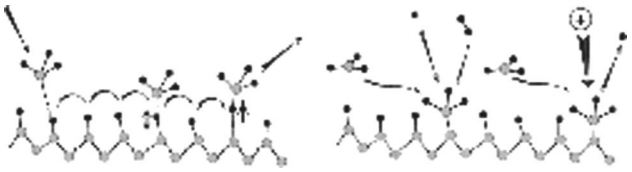

FIG. 5. Reaction kinetics of SiH_3 (left image) and CH_3 (right image) radicals with *a*-Si:H and *a*-C:H surfaces, respectively. SiH_3 is strongly physisorbed by the dipole interaction, whereas chemisorption of CH_3 is controlled by the creation of dangling bonds on the surface by either reactive hydrogen atoms or ion bombardment. From Perrin *et al.*, 1998.

bulk (Fig. 5, right). In this case, a heavy dilution of hydrocarbon gas feedstock in argon and/or hydrogen is frequently used to enhance the ion bombardment and hydrogen production. However, the energy of impinging ions should exceed the hydrogen abstraction energy, which in the case considered is approximately 0.34–0.4 eV (Frenklash and Wang, 1991). The ion energy should not be so high as to damage the ordered state of the substrate. We emphasize that the ability to activate the deposition surface while growing the building units is one of the unique features of reactive plasmas not common to thermal PECVD and other deposition systems. Other examples of the role of reactive plasmas in the preparation of solid deposition surfaces are given in Sec. IV.

Reactive plasmas and near-substrate sheath areas offer other useful features in the PECVD of nanofilms and nanostructures. We recall that two basic requirements for nanostructures and thin films are that the building units stick to the substrate only at the required sites (e.g., attach to an activated dangling bond or stick to the top of the growth island) and that they be able to migrate into place if inserted inappropriately. These two requirements place severe constraints on the process, simultaneously demanding strong and weak binding between the building units and the surface. By using the gas-phase transport of building units from reactive plasmas directly to the nanoassembly, one can diminish the importance of the "move into place" (over the surface) factor. This is particularly important for charged nanocluster and radical building units that can be driven and focused towards the target sites by sheath electric fields. For example, in the deposition of high-aspect-ratio nano-objects such as nanoneedles, nanotips, nanopyramids, or vertically aligned carbon nanotubes (some of these are discussed in Sec. IV), the electric-field lines converge towards the sharp ends of the nanostructures. The ion fluxes focused on sharp tips of individual nanostructures facilitate selective deposition and stacking of the building units. A representative example is shown in Fig. 6. Here the ion current density is distributed over the nanostructured surface in the PECVD of ordered arrays of carbon nanotip structures in $Ar+H_2+CH_4$ plasmas, computed via a hybrid fluid/Monte Carlo simulation (Levchenko and Ostrikov, 2005).

In the reactive-plasma-based systems, one can thus effectively remove the requirement of weak binding to the

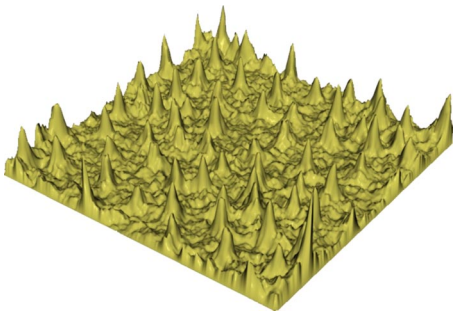

FIG. 6. (Color in online edition) Representative distribution of ion current density over a nanostructured surface in the $Ar+H_2+CH_4$ reactive-plasma-assisted nanofabrication of ordered carbon nanotip arrays for electron-field emission applications. From Levchenko and Ostrikov, 2005.

substrate and focus on the enhancement of binding to the nanoassembly upon landing. Various weakly adhesive buffer layers are often used in nanoassemblies to speed up the surface diffusion and promote coalescence of adatoms into 3D clusters (Poole and Owens, 2003; Shchukin *et al.*, 2003). In a sense, the plasma also acts as a buffer layer, where nanocluster building units can coalesce, be electrostatically charged, and then be transported directly to the required nanoassembly in a weakly collisional environment. In this regard, electrostatic charge prevents the plasma-grown nanocluster building units from further coalescence in the gas phase or on the surface, which is ideal for fabrication of high-quality films and nanostructures (Hwang and Kim, 2004).

An interesting point is that maintaining the charge in nanocluster unit-based deposition processes usually prevents undesired coagulation/agglomeration in the gas phase. This is particularly important for the synthesis of perfectly crystalline films using nanosized building units. In addition to charges owing to specific chemical and electronic structures of the nanoclusters/nanocrystals (Baron *et al.*, 2001), continuous microscopic currents of the plasma electrons and ions (usually negligible in thermal CVD processes) also contribute to the charging process (Vladimirov and Ostrikov, 2004). When the clusters approach very close to the surface (distances of the order of a_c, where a_c is the nanocluster size), further deposition critically depends on the charging state of the surface and the relative conductivity of the gas phase and the surface. In thermal CVD systems, charged nanoclusters land differently on conducting and insulating substrates, which results in selective deposition, especially when the gas phase is insulating (Hwang and Kim, 2004). This different behavior is attributed to different charge-transfer rates of insulating and conducting surfaces. If a cluster approaches a conducting surface, the cluster's charge is easily dissipated during the deposition, and the surface remains charge neutral. On the other hand, dielectric surfaces poorly dissipate the charge and remain charged. In this case, nanoclusters with the same charge polarity as the substrate have difficulty in landing. However, if the clusters are large enough, strong (short-

range) polarization effects can diminish the (long-range) Coulomb repulsion and enable the deposition. Thus smaller nanoclusters experience more difficulties in landing on insulating surfaces and are ideal to increase the selectivity of deposition. It is notable that in thermal CVD systems high substrate charge-transfer rates usually result in porous, skeletal, cauliflower, etc., structures that emerge as a result of coalescence of neutral clusters on the surface. Conversely, in situations when the charge-transfer rates are low and the building unit sizes are small, perfect and highly compact 3D assemblies and, eventually, dense films can be synthesized.

In PECVD, the gas phase is highly conductive and is favorable for efficient cluster charge dissipation upon contact with either insulating or conducting surfaces. Moreover, as has been mentioned above, the substrates are usually charged negatively at the initial stage of deposition and remain negatively charged if the charge dissipation in conducting substrates is efficient. This favors the deposition of positively charged nanoclusters and nucleates. However, when an insulating material is deposited, the charge is predominantly dissipated through the ionized gas phase. Therefore the plasma provides "equal opportunities" for deposition on insulating and conducting substrates and is generally believed to be detrimental to selective deposition (Tsubochi and Masu, 1992). However, as discussed above, selective deposition of various building units onto specific substrate areas with different surface morphology can be efficiently controlled by self-sustained nonuniform sheath electric fields, which is impossible in thermal CVD systems without any external substrate bias.

It is interesting to note that one can still synthesize high-quality closely packed assemblies in the reactive plasmas, despite very high charge-transfer rates in the ionized gas phase. A possible explanation would include two factors. First, the importance of reactive radical building units is much higher in PECVD than in thermal CVD. Second, if the nanocluster deposition is dominant, it is likely that while "burrowing" into the substrate exposed to the plasma, the nanocluster building units dissipate their original charge acquired in the gas phase and adopt the (usually negative) equilibrium charge of the local area at the substrate. Thus the clusters remain charged when coming into contact with the substrate, which prevents them from coalescing on the surface, as would happen in thermal CVD systems with substrates having high charge-transfer rates. Thus it is generally advantageous to use plasma-based CVD for depositing high-quality films on substrates with high charge-transfer rates. The benefits of selective deposition in thermal CVD systems are not so obvious because of larger numbers of neutral clusters (than in PECVD systems), which tend to agglomerate in the gas phase to form porous skeletal or cauliflower structures.

The ability to support ordered assemblies of certain building units in the gas phase via long-range electrostatic interactions is yet another distinctive feature of the plasma environments. For example, plasma-grown or externally dispensed negatively charged grains (typically in the sub-μm and μm size range) suspended in the near-sheath areas, can form ordered lattices commonly called *Coulomb* (or *dust*) *crystals* (Thomas and Morphill, 1996; Merlino and Goree, 2004). Such stable arrangements of the building units could, in principle, be used for fabrication of ordered arrays of fine particles on the surface or epitaxial recrystallization on prepatterned substrates (with the pattern size matching the lattice constant of the Coulomb crystal). However, these possibilities still remain to be realized.

To conclude this section, we mention that one can achieve reasonably high deposition rates (of the order of a few nm/s) in PECVD of various nanoassemblies, which can be enhanced by controlling near-substrate electric fields and using positively charged radical, nanocluster, or small nanoparticle units. In typical thermal CVD systems, growth rates in excess of 100 nm/h usually cannot be supported by the atomic/molecular building units. Therefore these systems rely entirely on nanocluster building units (Hwang and Kim, 2004).

IV. SPECIFIC NANOFABRICATION PROCESSES

In this section, we shall discuss some of the most common nanoassemblies and nanofilms from the viewpoint of the four-tiered "cause and effect" approach. Specifically, we shall look at the issues of generation and transport of building units, surface preparation, and elements of growth kinetics.

A. Semiconducting nanofilms and nanostructures

Nanostructured silicon thin films are widely used today for applications in solar cells. Various modifications of such films are commonly fabricated by using silane-based reactive plasmas. Even though silicon thin-film technologies offer great potential for economically viable solutions in mass production, the share of thin films (currently dominated by hydrogenated amorphous silicon *a*-Si:H) in the photovoltiac market still remains quite low due to a number of unresolved issues, such as low deposition rates, relatively high production cost, the conflictory requirements of minimal film thickness and maximal solar energy absorption, and the need for improvement of photostability and power generation efficiency. Recently, it has been shown that inclusion of nm-sized Si or Si:H crystallites ("cause") greatly improves performance of *a*-Si:H films in solar cell application ("effect"). In particular, by developing device-grade *pm*-Si:H films, it appears possible to improve transport properties, reduce photoinduced degradation, control the energy band gap, minimize the film thickness, and achieve very high deposition rates (exceeding 5 nm/s; Tanda *et al.*, 2003; see also Viera *et al.*, 2002; Roca i Cabarrocas *et al.*, 2004).

The plasma-nucleated nanocrystalline building units are very likely the cause of these remarkable improvements in film performance, although the mechanisms for their successes are not fully understood. There is thus

strong incentive to figure out how to generate them and incorporate them into the films according to the four-step nanofabrication scenario.

Silane-based reactive plasmas have shown a remarkable ability to generate a large number of reactive radicals and support gas-phase polymerization of macromolecules and generation of critical clusters (Perrin and Hollenstein, 1999; Hollenstein, 2000). A cluster formation pathway is dominated by anion-neutral reactions, commonly referred to as the *Winchester mechanism* of ion-molecular cluster growth (Bhandarkar *et al.*, 2000; Fridman and Kennedy, 2004). The essence of this mechanism is the thermodynamic advantage of the anion-induced clustering. A typical anion-supported clustering process,

$$Si_nH_{2n+1}^- + SiH_4 \rightarrow Si_{n+1}H_{2n+3}^- + H_2,$$

involves the sequence of silyl anions,

$$SiH_3^- \rightarrow Si_2H_5^- \rightarrow Si_3H_7^- \rightarrow \cdots \rightarrow Si_{n+1}H_{2n+3}^-,$$

with electron affinities $\mathcal{E}_a^n$ increasing with the number of silicon atoms in the cluster and reaching the work function of bulk hydrogenated silicon. Thus each reaction step is exothermic. More importantly, exothermic anion-molecular reactions usually have no activation barrier and feature very high rates. This fundamental conclusion explains the dominance of anion-induced clustering of Si:H and has recently been confirmed by numerical simulations of particle generation mechanisms in silane-based discharges (Suh *et al.*, 2003; De Bleecker *et al.*, 2004). In fact, over 90% of the critical cluster formation in silane reactive plasmas proceeds through the silyl anion pathway triggered by the SiH_3^- anion, whereas only about 10% proceeds through the siluene anion ($Si_nH_{2n}^-$) pathway, initiated by SiH_2^- (De Bleecker *et al.*, 2004).

One can thus conclude that the best strategy for generating the required building units is to optimize the nanoparticle-loaded discharge operation (Denysenko *et al.*, 2003; Ostrikov *et al.*, 2003) to enhance the gas-phase reactions leading to generation of SiH_3^- and SiH_2^- nanocluster precursors. This can be done via tailoring of the electron energy distribution function that controls most of the gas-phase reaction rates and hence the balance of reactive species in the discharge (Sugai *et al.*, 2001). However, at this stage it is crucial to ensure that critical clusters nucleate into the nanosized crystalline particles that are actually required for the PECVD of device-grade silicon films. A potential danger arises when the number densities of the primary nucleates exceed a certain threshold for triggering an (in most cases uncontrollable) agglomeration process. This condition is usually referred to as the onset of *powder generation* (Fridman *et al.*, 1996). The powder particles usually have complex fractal, cauliflower, porous skeletal, etc., shapes and typically exceed 40–50 nm in size (Perrin and Hollenstein, 1999; Hollenstein, 2000). Needless to say, such particles are detrimental for nanofabrication of *pm*-Si films and should be avoided.

Thus the nanofabrication of solar-cell-grade Si films should be based on generation of nanocrystalline building units away from powder generation conditions. For example, high-quality *pm*-Si films have been successfully deposited in rf plasmas of highly diluted $SiH_4(2\%) + H_2(98\%)$ gas mixtures at relatively high deposition temperatures ($\sim 200\,^\circ$C), deposition pressures (1.23 Torr), and rf input powers (~ 0.11 W/cm^3; Roca i Cabarrocas *et al.*, 1998). Under such conditions, heavy dilution of silane in hydrogen is beneficial for the growth of the *a*-Si:H matrix by SiH_3 radical building units via the hydrogen-mediated surface activation mechanism discussed in Sec. III. We emphasize that this PECVD regime is built upon selective deposition of the first population of small (1–2 nm) particles appearing in the ionized gas phase well before the onset of coagulation (Viera *et al.*, 2002). Transport of such building units to the substrate critically depends on their charge, on the distribution of gas temperature in the near-substrate areas, and on other conditions.

In a series of elegant recent experiments, the nature and charge of building units have been related to the surface roughness, damage, structure, and phase composition of Si:H films. For example, surface roughness progressively increases with the size of the building units, being ~ 2 nm when atomic/molecular units are used to build microcrystalline silicon films, ~ 4–5 nm when the contribution of plasma-grown nanocrystals is significant, and ~ 10 nm under powder-generating conditions (Chaabane *et al.*, 2003, 2004; Roca i Cabarrocas *et al.*, 2004). To study transport and the contribution of nanocrystalline building units to the silicon film properties, an independently biased "triode" mesh was placed in front of liquid-nitrogen-chilled ($T_s \sim 80$ K) substrates, as shown schematically in Fig. 7 (Chaabane *et al.*, 2004; Roca i Cabarrocas *et al.*, 2004). Physically, this arrangement substantially reduces contributions from surface migration of atomic/molecular building units and allows one to control the impact energies of small (1–2 nm) positively charged, plasma-grown nanocrystals. In this series of experiments the potential in the plasma bulk was ~ 25 V. Thus by applying a positive potential of +25 V one effectively reduces the landing energy of the building units almost to zero [Fig. 7(a)]. Under such conditions, Raman spectroscopy revealed that the films were purely crystalline, which implies that the building units landed in a perfectly nondestructive fashion. When the mesh potential was reduced to zero or negative values, the impact energy, and hence the disintegration probability effectively increased, and, as a result, so did the amorphous phase content. We recall that the amorphous phase predominantly grows by radical/molecular building units. In fact, when the mesh bias was reduced to -50 V, the amorphous phase content increased to almost 100%, reflecting complete breakdown of nanocrystalline building units into atomic/radical fragments, as schematically shown in Fig. 7(b). This behavior has also been confirmed by the results of molecular dynamics simulations of the landing of small nanoparticles on vari-

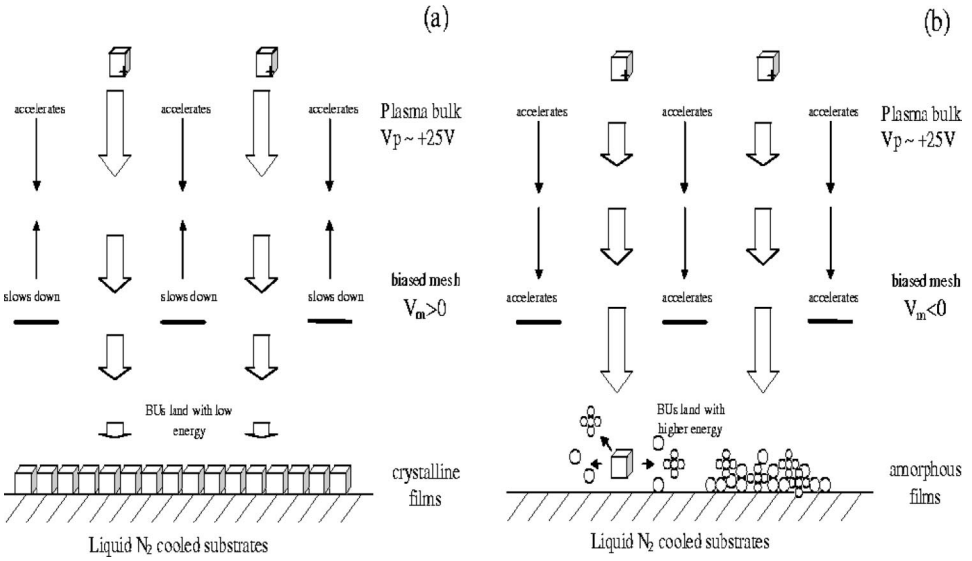

FIG. 7. Schematics of experiment on reactive-plasma-based deposition of positively charged nanocrystals onto liquid-nitrogen-cooled substrates (Chaabane *et al.*, 2004; Roca i Cabarrocas *et al.*, 2004): (a) When the building units (BUs) land with very low energy, there is no nanocluster disintegration and the films are predominantly crystalline; (b) when the building units are accelerated to higher energies, nanocrystals break up into atomic/radical fragments and the films are mostly amorphous.

ous substrates under similar deposition conditions (Roca i Cabarrocas *et al.*, 2004).

Another way to control the deposition dynamics of small nanoparticles is to use a gas temperature-gradient-driven thermophoretic force (Shiratani *et al.*, 2000; Fontcuberta i Morral and Roca i Cabarrocas, 2001). For example, when the substrates are externally heated, gas temperatures near the surface are usually higher than in the plasma bulk. In this case, nanoparticles are effectively pushed away to the plasma bulk and eventually to the pump line. By using the thermophoretic manipulation of larger (>1 nm) building units, one can enhance the probability of film growth predominantly by atomic/molecular units.

The fourth stage in our logical framework is the incorporation of the building units into the nanostructured film. Under heavy dilution conditions, the amorphous matrix grows with a rate comparable to that of the nanocrystalline building units that embed into it. This has been confirmed by high-resolution TEM (Viera *et al.*, 2002), which suggests that while the nanocrystalline building units grow in the gas phase, the *a*-Si:H matrix forms the lowest layer in the structure. Subsequent layers contain 1–2 nm nanocrystalline inclusions, as suggested by sharp and intense rings superimposed on diffuse rings in selected areas of electron diffraction patterns, indicating the presence of ordered structures in an amorphous matrix.

It is important to note that there is a tradeoff between the particle/film growth rates and particle crystallinity. In fact, despite much higher particle growth rates (~100 times), crystalline nanoparticles are very rarely observed in pure silane plasmas (Costa, 2000). As a remedy, one can use an alternative approach based on initial growth of amorphous and irregular-shaped particles and their subsequent annealing in hot working gas mixtures of silane and an inert gas (Bapat *et al.*, 2003). However, efficient annealing of nanoparticles requires very high working gas temperatures, often exceeding 1000 °C. Another issue is to minimize the size of crystalline building units generated by this production technique (20–80 nm) to at least 10 nm, which would warrant their applications in floating gate memory devices (Ostraat *et al.*, 2001).

We note that simultaneous integration of various building units in the same nanoassembly or nanostructured object can be very attractive for some applications. For example, by using $SiH_4+CH_4+H_2$ gas mixtures, one can grow polymorphous hydrogenated silicon carbide (*pm*-$Si_{1-x}C_x$:H), ideal for applications as a *p*-type nanolayer in PIN solar cells (Roca i Cabarrocas *et al.*, 2004). By varying the process parameters to adjust relative production of silicon- and carbon-bearing building units, one can control the value of x. Sputtering of atomic and nanocluster building units from multiple targets in the environments of reactive plasmas offers a further way to control the development of nanoassemblies with the desired properties. For example, concurrent rf magnetron sputtering of Al and In targets in reactive low-pressure discharges in nitrogen can be used to synthesize $Al_xIn_{1-x}N$ quantum dot structures and order them uniformly over large substrate areas [Fig. 8(a); Xu, Ostrikov, *et al.*, 2005]. By varying the rf power supplied to Al and In sputtering targets, one can control the release of aluminum- and indium-containing building units to the ionized gas phase and, eventually, the relative elemental composition $x/(1-x)$ of Al and In in the films. In this way, one can control the size of the individual quantum dots and the energy band gap of quantum dot structures in the range from ~6.2 eV (AlN, $x\approx 1$) to ~3.55 eV (InN, small x). This has been confirmed by the photoluminescence spectra of $Al_xIn_{1-x}N$ structures

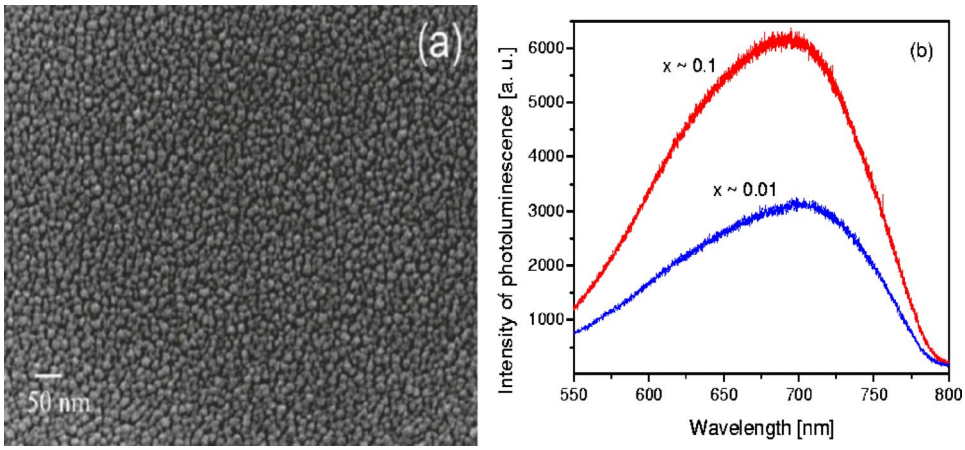

FIG. 8. (Color in online edition) Quantum dot deposition and emission properties: (a) Scanning electron micrograph of $Al_xIn_{1-x}N$ quantum dot structures synthesized by the reactive-plasma-assisted rf sputtering deposition technique; (b) dependence of the photoluminescence intensity on quantum dot size/composition (Xu, Ostrikov, *et al.*, 2005). Quantum dot size is smaller for smaller values of x.

shown in Fig. 8(b) which exhibit a notable blueshift of the photoluminescence maximum as x and the size of the quantum dot decrease (Xu, Ostrikov, *et al.*, 2005).

Figure 9(a) shows silicon nanowires synthesized in low-pressure (<100 mTorr) reactive plasmas of SiH_4+H_2 gas mixtures in the presence of a Ni catalyst (Ostrikov *et al.*, 2005). These nanoassemblies have outstanding potential for the development of molecular nanoelectronic devices. They were previously synthesized by charged nanocluster building units in thermal CVD systems (Hwang *et al.*, 2000). The assembly of very-high-aspect-ratio (1D) silicon nanowires can be explained by selective attraction of nanoclusters to the open end of 1D structures, schematically represented by rods in Fig. 9(b). In this example, both the rod and the building unit are positively charged, although the opposite can be the case in reactive plasmas. If the cluster approaches from the side [Fig. 9(b), left image], positive charges in the rod are repelled. However, since the diameter of silicon nanowires is very small [it does not exceed a few tens of nm in Fig. 9(a)], the nanorod-cluster interaction still remains repulsive. When the cluster approaches the nanowire from its growth end [Fig. 9(b), right image], positive charges are repelled to the opposite side of the rod, which results in an attractive electrostatic interaction between the cluster and nanowire and hence one-dimensional nanowire growth (Hwang and Kim, 2004). Thus the reactive-plasma-assisted growth of silicon nanowires has an outstanding potential for controlling the direction of growth. Efforts should be made to investigate similar control of crystallographic growth direction recently achieved by the metal-organic CVD technique (Kuykendall *et al.*, 2004).

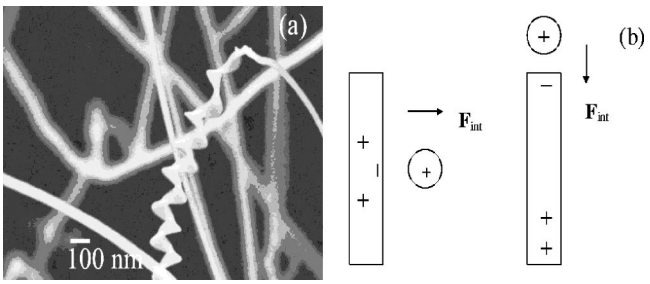

FIG. 9. Silicon nanowire growth and interaction with charged clusters: (a) Scanning electron micrograph of silicon nanowires grown in low-pressure SiH_4+H_2 reactive plasma (Xu, Ostrikov, *et al.*, 2005); (b) schematics of the charged nanocluster-nanowire interaction (Hwang and Kim, 2004). Here, $\mathbf{F}_{int}$ denotes the force of the electrostatic building-unit–nanowire interaction.

B. Carbon-based nanostructures

Various carbon-based nanostructures can be grown in reactive plasmas made up of mixtures of carbon-carrier gases (e.g., hydrocarbons C_xH_y, fluorocarbons C_xF_y, fullerenes, etc.) with other functional feedstock (H_2, NH_3, inert gases, etc.). We emphasize that in the "cause and effect" framework, the choice of working gases and process parameters should be driven by the required building units, surface preparation, and specific transport and stacking requirements.

Here, we focus on a few typical examples of carbon-based nanostructures fabricated in reactive plasma systems, such as carbon nanoparticles, nanotips, nanotubes, nanowalls, and ultrananocrystalline diamond. With regard to these carbon nanostructures, the most commonly invoked building units are carbon dimer C_2 (Gruen, 2001), graphitic nanofragments (Louchev and Hester, 2003), charged nanoclusters (Hwang *et al.*, 1996; Hwang, 1999; Hwang and Kim, 2004), and carbon nanoparticles (Gebauer and Winter, 2003; Hong *et al.*, 2003; Kovacevic *et al.*, 2003). Some other atomic and radical species have also been discussed extensively as mediators of clustering and film growth processes. As for fabrication of nanostructured films in silane-based reactive plasmas, discussed in the previous section, nanoparticles

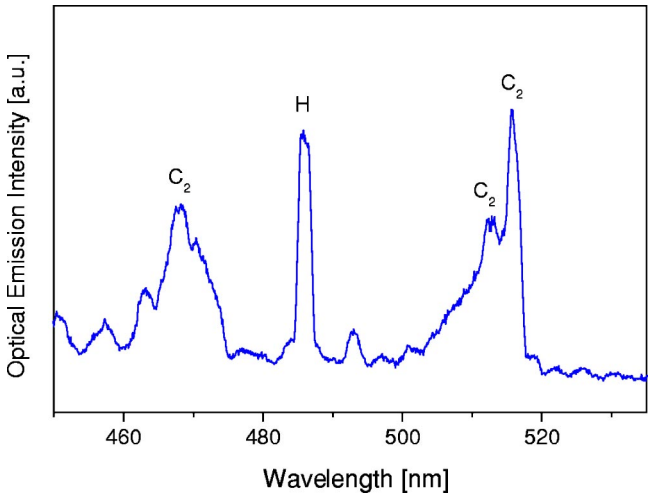

FIG. 10. (Color in online edition) Characteristic optical emission lines of the carbon dimer in nanofabrication of carbon nanowall-like structures in $Ar+C_2H_2+H_2$ rf plasmas (Long *et al.*, 2005).

larger than a few tens of nm are usually of limited interest for most common nanoassemblies. It has been suggested that various graphitic nanofragments could control the assembly of carbon nanotubes (Louchev and Hester, 2003). In reactive plasma environments, graphite nanofragments can appear as a result of decomposition of larger carbon nanoparticles in the discharge or sputtering of graphite substrates. However, the existing knowledge on generation of these fragments in reactive plasmas is limited and will require further research.

The abundance of carbon dimer and carbon nanocluster building units, as well as other important species (e.g., growth precursors and mediators), in reactive plasma systems can be predicted by numerical modeling that takes into account ion-induced clustering in the ionized gas phase (Stoykov *et al.*, 2001; Denysenko *et al.*, 2004; Gordillo-Vazques and Albella, 2004). In particular, in rf plasmas of C_2H_2 highly diluted in argon, number densities of the carbon dimer in two excited states $X^1\Sigma_g^+$ and $a^3\Pi_u$, are higher at lower working gas pressures and argon concentrations (Gordillo-Vazques and Albella, 2004). Another powerful tool in monitoring the discharge species is optical emission spectroscopy. The strongest emission lines of carbon dimer C_2 generated in low-pressure (20–40 mTorr) rf plasmas of an $Ar(75\%)+H_2(10\%)+C_2H_2(15\%)$ gas mixture are shown in Fig. 10. Peaks like those in the figure can be used to trace the appearance of carbon dimers in various situations. Surprisingly, the strongest peak, located at ~516.5 nm, is also seen in the Swan-band visible absorption spectra of numerous protoplanetary nebulae, implying a possible important role of the carbon dimer in the evolution of red-star–protoplanetary systems (Hrivnak and Kwok, 1999).

Knowledge of the number densities of other (e.g., C_xH_y) neutral and charged species is indispensable for the improvement of control strategies. For example, the radical species CH_3 has been suggested in Sec. III.C as a building unit in the growth of *a*-C:H films (Perrin *et al.*, 1998). Atomic hydrogen is also of interest, since it is able to activate surface carbon bonds and simultaneously etch the amorphous carbon phase. Number densities of numerous charged and neutral species in CH_4+H_2+Ar high-density reactive plasmas can be found elsewhere (Denysenko *et al.*, 2004).

The most likely mechanism of carbon clustering in C_2H_2-based plasmas is quite similar to the Winchester mechanism of silicon hydride clustering and also involves the chain

$$C_iH_j^- + C_mH_n \rightarrow C_{i+m}H_{j+n-1}^- + H,$$

of anion-neutral clustering that proceeds via extraction of hydrogen and generation of higher anions (Stoykov *et al.*, 2001). Furthermore, the carbon dimer C_2, featuring high electron affinity, can attach a plasma electron and become anionic C_2^-. This highly reactive radical has also been suggested as a possible trigger of anion-neutral clustering (Hwang and Kim, 2004). Relevant modeling results (which include charge neutralization, neutral clustering, diffusion loss of the plasma species, and other effects) suggest that larger C_mH_n clusters with $m>10$ are negatively charged at higher gas temperatures and lower degrees of ionization and operating pressures (Stoykov *et al.*, 2001). Otherwise, one should expect a pronounced generation of neutral or positively charged nanoclusters. However, positively charged carbon-based clusters were not included in the clustering model (Stoykov *et al.*, 2001), thus warranting their explicit consideration in the near future.

Having identified potential building units and important process mediators in hydrocarbon-based reactive plasmas, let us turn now to surface preparation and activation. Many nanofabrication processes, such as growth of carbon nanotubes (Chhowalla *et al.*, 2001; Meyyappan *et al.*, 2003), require specially activated thin catalyst layers (e.g., Ni, Fe, Co) usually not exceeding a few tens of nm in thickness, which rearrange into individual nanoparticles on the substrate surface, as can be seen in Fig. 11(a). Such nanoparticles support precipitation and self-assembly of carbon building units into various nanostructures, such as single-walled or multiwalled carbon nanotubes, carbon nanotips [Fig. 11(b)], nanopyramids [Fig. 11(c)], nanowall-like structures [Fig. 11(d)], and several others. Activation of the growth surface is usually achieved by externally heating the substrate to temperatures that exceed the melting point of the catalyst layer, typically 500–600 °C and higher. It is notable that when the film thickness is in the nanometer range, the melting points are lower than those of the corresponding bulk materials (Poole and Owens, 2003). To ensure efficient bonding of the nanostructure to the substrate, one should ensure adequate wetting of the substrate by the catalyst nanoparticles. In this case, one would expect the "base" growth scenario. However, sufficiently intense ion bombardment (controlled by the substrate bias) contributes to the loosening of the catalyst nanoparticles, thus leading to the "tip" growth pathway. In this case, reactive-plasma-assisted techniques of-

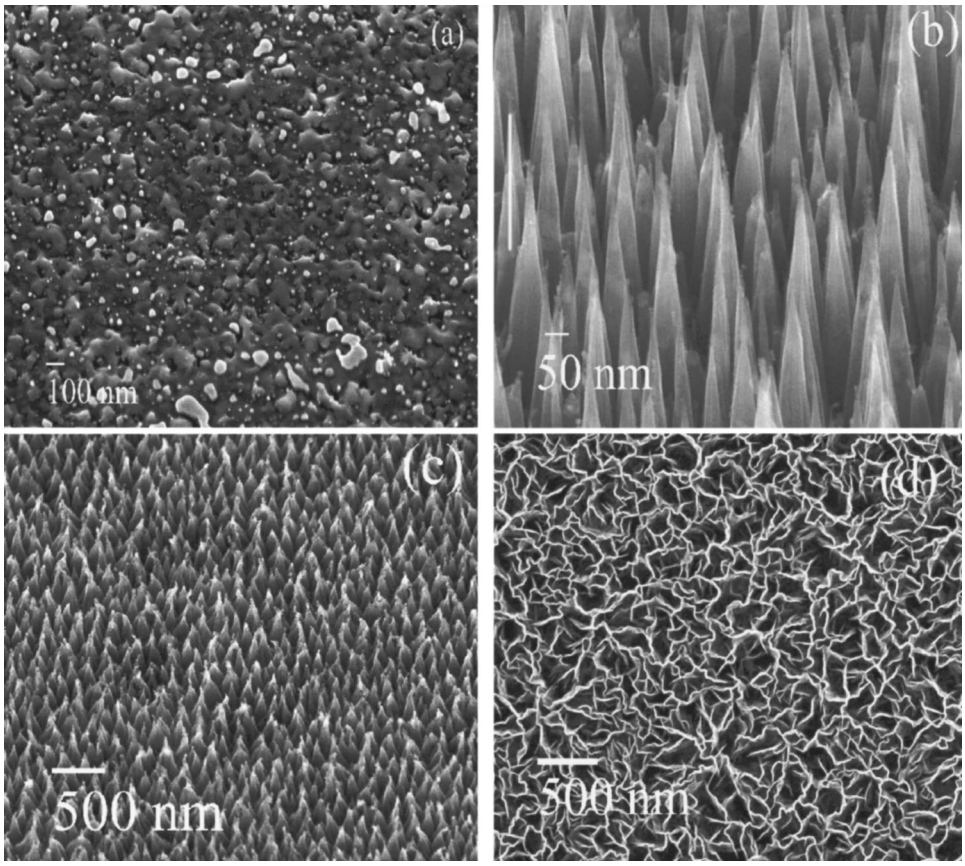

FIG. 11. Various carbon nanostructures synthesized in hydrocarbon-based reactive plasmas: (a) Ni-catalyzed Si(100) surface before the beginning of PECVD; (b) carbon nanotips; (c) pyramidlike structures grown in $Ar+CH_4+H_2$ plasmas without any external substrate heating; (d) carbon nanowall-like structures grown in $Ar+C_2H_2+H_2$ rf plasmas. (Figure courtesy of J. D. Long and Z. Tsakadze.)

ten produce individual, free-standing, vertically aligned multiwalled carbon nanotubes (Merkulov *et al.*, 2000; Hash and Meyyappan, 2003). This is one reason why PECVD techniques are more suitable for synthesizing multiwalled rather than single-walled carbon nanotubes (Meyyappan *et al.*, 2003), since the latter usually grow through the "base" growth mechanism.

Plasma environments offer additional options for activating catalyst layers. For example, the Ni-based layer in Fig. 11(a) was activated in low-pressure ~40 mTorr rf plasmas of $Ar+H_2$ gas mixtures by using intense fluxes of argon ions, reactive chemical etching of metal surface by hydrogen atoms, and heating by hot neutrals (with temperatures in the range 270–400 °C) (Tsakadze *et al.*, 2004, 2005). It is important to note that in some cases, such as the PECVD of nanopyramids in Fig. 11(c), it is not necessary to additionally heat the substrates externally, a situation quite uncommon for thermal CVD systems.

While catalyst nanoislands usually serve as the "base" for the growth of carbon nanostructures, other areas, uncovered by the carbon nanostructures, are subject to deposition of amorphous carbon. Thus the actual film growth process involves concurrent growth of two phases, one nanostructured and the other amorphous. To synthesize better-quality nanostructures (e.g., crystalline), one should thus inhibit the development of the amorphous phase and promote the growth of the nanoassemblies. Again, by invoking the cause and effect approach, we recall from Sec. III.C that efficient growth of *a*-C requires plasma-mediated activation of dangling bonds for the stacking of CH_3 radicals. On the other hand, preferential growth of the nanoassembly requires elevated abundance of highly reactive carbon dimers or suitable nanocluster building units in the gas phase. To this end, it would be beneficial to maximize production of C_2 and/or nanoclusters and minimize the presence of CH_3. An interesting way to maximize the production of carbon dimer molecules is to dissociate purely carbon feedstock, such as gaseous C_{60}, a carbon allotrope that is less stable than diamond or graphite. In fact, by using plasma-assisted techniques, one can achieve unusually high rates of conversion of the C_{60} feedstock into C_2 molecules (Gruen, 2001). Moreover, during the growth stage, reasonably high densities of hydrogen atoms are desirable for preferential chemical etching of the amorphous phase. However, the hydrogen content cannot be made very high without detriment to the growth process. For example, large amounts of hydrogen can re-gasify embryonic nuclei during the synthesis of nanocrystalline diamond (Gruen, 2001) and excessively activate carbon

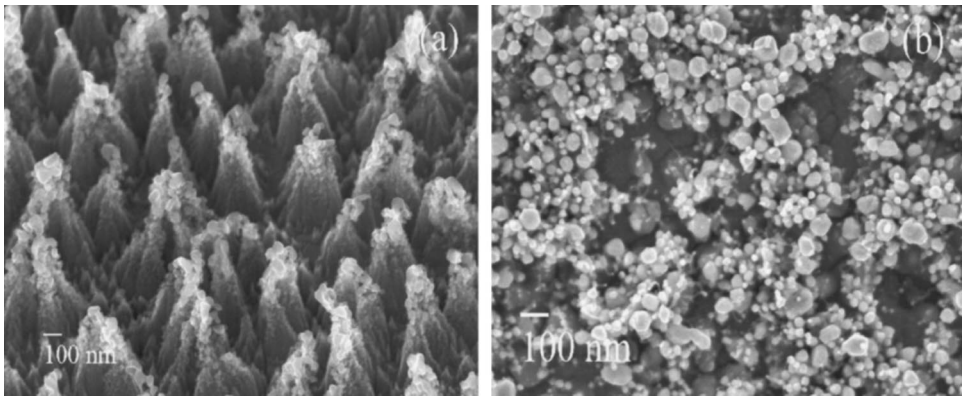

FIG. 12. Nanoparticles (a) attached to the top of carbon nanotip structures and (b) on a nickel-catalyzed silicon surface (Tsakadze *et al.*, 2004, 2005).

surface bonds required for the growth of *a*-C.

Using plasma-assisted nanofabrication methods, one should always keep in mind that the ion energy should be just sufficient for the desired surface activation. Extra strong ion bombardment can cause irremediable defects to the nanostructures being grown and also destroy some nanocluster building units in the gas phase. For example, energetic ions impinging on the growth surface can compromise the integrity and ordering of vertically aligned nanotube patterns. This situation can be remedied by applying strong magnetic fields (~2 T) parallel to the substrate (Hirata *et al.*, 2003) or reducing the near-substrate sheath potentials.

It is worthwhile to mention that transport of building units in hydrocarbon plasma environments has not yet attracted as much attention as similar research efforts on hydrosilicon plasmas (see Sec. IV.A). However, the existing modeling results can be used to estimate surface fluxes of numerous charged and neutral plasma species in the process of assembly of various carbon nanostructures (Hash and Meyyappan, 2003; Denysenko *et al.*, 2004; Gordillo-Vazques and Albella, 2004). Larger building units (e.g., larger nanoclusters or nucleates exceeding 10 nm) can be efficiently manipulated by using thermophoretic forces (Rutkevych *et al.*, 2004). Indeed, when Ni-catalyzed silicon substrates are not externally heated, fallout of gas-phase nucleated carbon nanoparticles is frequently observed. However, by externally heating the substrates under the same operating conditions, one imposes an additional temperature gradient and hence a thermophoretic force that can completely remove carbon nanoparticles from the surface. The resulting nanoparticle-free assemblies resemble the ordered carbon nanotip patterns in Fig. 11(b).

We now consider stacking of the building units into carbon-based nanoassembly patterns. The first example is the insertion of the carbon dimer C_2 into a dimer row on the reconstructed (100) surface of diamond (Gruen, 2001). Detailed density-functional calculations show that the insertion of one of the carbon atoms of a gas-phase carbon dimer molecule into the dimer rows of the reconstructed (100) surface leaves the other carbon dimer free to react with additional gas-phase carbon dimers to form a new diamond crystallite, which grows larger and eventually forms a grain boundary (Gruen *et al.*, 1999). Other examples of interactions of the carbon dimer with reconstructed (100) and (111) surfaces of diamond can be found elesewhere (Walch and Merkle, 1998). Notably, depending on surface hydrogenation and other factors, the hybridization of carbon dimers on the reconstructed surface may not necessarily reproduce the sp^3 hybridization in the bulk. Thus control of spontaneous reconstruction of carbon "dimer" surfaces is one of the current challenges of nanoscience. Specific chemical structure and the high reactivity of the carbon dimer have been argued to be major factors in the reactive-plasma-assisted fabrication of two-dimensional carbon nanostructures such as carbon nanowalls and nanowall-like structures [Fig. 11(d); Long *et al.*, 2005]. On the other hand, insertion of carbon into *a*-C films can be investigated by density-functional, tight-binding, and empirical simulation methods (Marks *et al.*, 2002, 2003).

Larger building units stack into carbon-based nanoassemblies quite differently. For example, small nanoclusters can epitaxially recrystallize in a manner similar to that discussed in Sec. III. However, larger nanoclusters and nucleates can be driven by focused electric fields and eventually stick to the top ends of high-aspect-ratio carbon nanotip structures [Fig. 12(a)]. In some other cases (e.g., unbiased substrates) the building units can fall out onto the substrate, as can be seen in Fig. 12(b). To aid in depositions, the top surface of the carbon nanotips can be flattened as a result of etching by intense ion fluxes (Tsakadze *et al.*, 2004, 2005), creating more secure spots for the building units to alight.

Thus, by adopting the cause and effect approach advocated in this Colloquium and following basic considerations during each of the nanofabrication steps, one can, in principle, grow, enhance, and perfect desired properties in various carbon nanostructures, such as single crystallinity of the carbon nanotips in Fig. 11(b). However, many important questions still remain open. For example, what is the cause of the pronounced vertical alignment of carbon nanotubes and carbon nanotips grown by plasma-assisted techniques? We recall that the

electric field **E** is nonuniform in the plasma sheath. It is focused on the growth spots from the initial stage, when the growth island forms (Levchenko *et al.*, 2004), and it drives the charged building units, facilitating their stacking into the nanoassembly directly from the gas phase. Meanwhile, strong electric fields in the vicinity of the nanotips polarize neutral (e.g., nanocluster) building units and align them to stack in the nanoassembly, with a higher probability of approaching from the top. Unidirectional precipitation of both charged and neutral building units favors the assembly of the structures along the direction of **E**, on a unit-by-unit basis. However, stacking of neutral building units with poor polarization response does not necessarily happen in the direction of **E**. In this case the electrostatic force creates stress that is nonuniformly distributed over the interface between the catalyst nanoparticle and the carbon nanotube structure. As a result, precipitation rates become different in areas with different stress, and vertical growth is dynamically maintained (Merkulov *et al.*, 2001). However, how this nonuniformity of stress translates specifically into preferential stacking of the building units still requires an adequate explanation. Another open question is why the carbon nanotubes grown via the "tip" mechanism are multiwalled (the only kind of carbon nanotubes grown in reactive plasmas), whereas the base-grown ones are single-walled (Meyyappan *et al.*, 2003). In this regard, one should take into account that the assembly of single-walled nanotubes requires a low supply of carbon to the catalyst particle surface and suppression of higher hydrocarbons (Kanzow and Ding, 1999), conditions that are quite difficult to meet in reactive-plasma-assisted processes.

Recent results of atomic-scale *in situ* TEM imaging of carbon nanofiber growth suggest that multiple graphene sheet-made nanofiber walls are formed at monoatomic step edges at the C-Ni interface (Helveg *et al.*, 2004). The steps continuously develop and disappear while an initially fairly spherical nickel catalyst particle attached to the $MgAl_2O_4$ surface periodically elongates, reshapes, and eventually contracts to a spherical shape. The growth terminates when the graphene sheets encapsulate the Ni particle completely, indicating that metal-gas interaction is essential for nanofiber growth. If this process were conducted in a plasma environment, one would expect that electrostatic interactions between the (usually negatively) charged catalyst nanoparticle and substrate surface could facilitate dynamic reshaping of the particle and its detachment from the surface. This effect has previously been used for electrostatic shedding of fine powder particles from solid surfaces in plasma discharges (Goree and Sheridan, 1992) and can be invoked for the explanation of predominant tip-growth of multiwalled carbon nanostructures in a plasma.

From the above considerations, one can conclude that reactive-plasma-assisted techniques offer advantage over thermal CVD when at least one of the following is required:

(i) control of densities and fluxes of the required building units in the gas phase, which is difficult (if possible at all) to do on the surface of catalyst nanoparticles (e.g., in growth of carbon nanotubes);

(ii) electric-field-guided delivery of the building units straight to the nanoassembly from the ionized gas phase;

(iii) specific substrate activation by ion/heat fluxes from the gas phase;

(iv) preferential growth and alignment direction, such as the direction of the sheath electric field.

Nonetheless, the actual role of the plasma in the growth of carbon nanotubes is still a subject of intense discussion within the research community. The most widely accepted view is that since the dissociation of precursor gas on the surface of catalyst particles is sufficient for carbon material precipitation, the ability of the plasma to dissociate the gas feedstock into reactive radicals should not be a factor in the growth of carbon nanotubes (Meyyappan *et al.*, 2003). Here, one should clearly understand the consequences of additional dissociation of the feedstock gas in the plasma. Extra radical building units produced in the gas phase reduce the need for their production on the catalyzed surface. Thus this process is energetically favorable and could be one of the reasons for the lower substrate temperatures required to synthesize carbon nanostructures by plasma-assisted methods. Another argument in favor of the importance of the gas-phase decomposition of working gas is the possibility of plasma-assisted growth of multiwalled carbon nanotubes without a catalyst (Obraztsov *et al.*, 2000; Tsai *et al.*, 2000). It is indeed likely that carbon-carrying building units could precipitate into nanoassemblies directly from the gas phase. Another interesting point is that the CVD of carbon nanotubes usually requires substrate temperatures of at least 550 °C, and the cold wafer scenario is quite unlikely (Meyyappan *et al.*, 2003). With the use of reactive plasmas, growth temperatures of carbon nanotubes as low as 120 °C have been reported (Hofmann *et al.*, 2003). Furthermore, various carbon nanostructures can be grown in reactive plasmas without any external heating of the substrate (Tsakadze *et al.*, 2004, 2005). In this case, the neutral component of the weakly ionized plasma environment is responsible for heating of the catalyst layer.

To conclude this section, we note that more efficient species generation and plasma polymerization generally require higher chemical activity of the gas feedstock. Thus using highly reactive gases such as ethylene, acetylene, or propylene is considered beneficial in enhancing the process yield. For example, nanoparticle generation and nanostructure growth is more efficient in acetylene-based than methane-based plasmas (Hong *et al.*, 2003; Xu, Ostrikov, *et al.*, 2005).

C. Other nanofabrication processes

The synthesis of silicon- and carbon-based nanoassemblies discussed in the previous sections are the most widely studied plasma-aided nanofabrication processes. In this section, we shall outline some other examples of the use of reactive plasmas for various nanoscale assemblies and comment on them within the framework of the "cause and effect" approach.

The first example is the growth of charged nanocluster building units in the ionized gas phase and their use for plasma-assisted dc magnetron reactive sputtering deposition of highly crystalline TiO_2 films on unheated substrates (Barnes *et al.*, 2004, 2005). This technique is based on the charged-cluster theory (Hwang and Kim, 2004) discussed in Sec. III and is successful for high-quality crystalline film deposition subject to meeting the following conditions: (i) small (typically 1–3 nm) amorphous-liquid-like nanoclusters are generated in the gas phase; (ii) the clusters are charged in the plasma; (iii) the charge is efficiently dissipated upon deposition. Some of these factors have already been discussed above in a different context. In this example, the first requirement is essential for epitaxial recrystallization of small nanoclusters with nonfixed crystalline structure and lower melting points. The charged state is crucial to prevent gas-phase cluster agglomeration, and charge dissipation is necessary to avoid undesired charge buildup on the substrate surface.

TiO_2 nanoclusters were generated in the ionized-gas phase of $Ar+O_2$ mixtures under low-pressure conditions and collected by carbon-coated copper TEM grids positioned at different distances (50–250 mm) from a Ti sputtering target, then imaged by the TEM (Barnes *et al.*, 2004, 2005). Interestingly, the clusters collected closer to the sputtering target (at 50 nm) were considerably smaller than those captured on the grid located 250 nm away from the target. The closer grid had clusters less than 2 nm in size and containing ~400 atoms, while the more distant clusters measured more than 3 nm in size and contained ~1400 atoms. This implies that clustering occurs in the gas phase and continues as the nanocluster building units are transported towards the deposition substrate. Hence one should be able to control the size of the building units by moving the (electrically floating) substrate towards and away from the sputtering target. Specifically, smaller clusters produce faceted crystalline anatase film, whereas larger clusters result in mostly amorphous films (Barnes *et al.*, 2004, 2005). This result is consistent with the size-dependent phase composition of TiO_2 clusters, with the amorphous-to-crystalline transition in the size range between 1.5 and 3 nm (Monticone *et al.*, 2000). We note that the value of the dc power does not significantly affect the cluster generation and film properties. However, rf power strongly affects the building-unit-based synthesis of TiO_2 films in $TiCl_4+O_2$ parallel-plate rf plasmas (Barnes *et al.*, 2003). Indeed, the nanocluster size, charge, and film structure change with the variation in rf power input. At low rf (~90 W), the films resemble random fractal and agglomerated structures and can be easily removed from the substrate. However, at higher powers (~180 W), the films are better ordered, denser, and feature higher crystalline phase content. Note that the different effects of the input power in the two plasma-assisted sputtering processes (Barnes *et al.*, 2004, 2005) and in PECVD (Barnes *et al.*, 2003) reflect the higher reactivity of titanium tetrachloride-based reactive plasmas, a major factor in the generation of TiO_2 nanocluster building units. Furthermore, the sizes of the building units were different at different input powers, 10–15 nm at 90 W and 7–12 nm at 180 W (Barnes *et al.*, 2003). Nanocluster agglomeration observed at 90 W, which was attributed to different charging efficiency of the reactor, can be avoided by operating the discharge in the higher-power mode. Future research efforts on this phenomenon should involve comprehensive modeling of the nanocluster formation and charging process in the experiments concerned (Barnes *et al.*, 2003, 2004, 2005). Knowledge of the nanocluster charge would shed some light on the actual role of reactive plasmas in assembling highly crystalline TiO_2 films.

The elegant approach of Barnes *et al.* (2003, 2004, 2005) can be used for direct *in situ* sampling and characterization of small (in the few-nm size range) nanoclusters in the ionized-gas phase. Because of the extremely small sizes of the nanoclusters involved, such sampling is one of the most difficult challenges faced today in the study of nanoclustering. Some other (mostly indirect) methods of nanocluster detection and characterization in the plasma have been presented elsewhere (Boufendi *et al.*, 1999; Ghidini *et al.*, 2004).

Another interesting example of how different building units in different plasma environments can result in totally different properties of nanofilms is the plasma-assisted fabrication of hydroxyapatite (HA) bioceramic coatings on Ti-6Al-4V orthopedic alloys, widely used by the biomedical industry for hip joint and dental implants. The HA coating is used to improve biocompatibility of the implants, sustain remodeling of bone tissues, ensure stronger implant fixation, suppress undesirable inflammatory responses, and dramatically shorten healing times (Sun *et al.*, 2001). One of the most commonly used methods of depositing HA bioceramic coatings on implant alloys is thermal plasma spraying (Klein *et al.*, 1994; Tsui *et al.*, 1998). This method uses thermal plasma jets carrying microdispersed hydroxyapatite powder building units towards the deposition surfaces. However, despite its apparent simplicity, moderate deposition rates, and relatively low cost, this technique is unlikely to meet current industrial standards (ASTM, 2003). This is because, under typical operating conditions, micron-sized HA powder building units usually land on the metal surface without any significant decomposition into smaller fragments. As a result, hydroxyapatite bioceramics prepared by the plasma spray method are mostly amorphous and feature highly porous structure and irregular surface morphology with surface roughness in the submicrometer range (Klein *et al.*, 1994; Tsui *et al.*, 1998). This ultimately leads to very

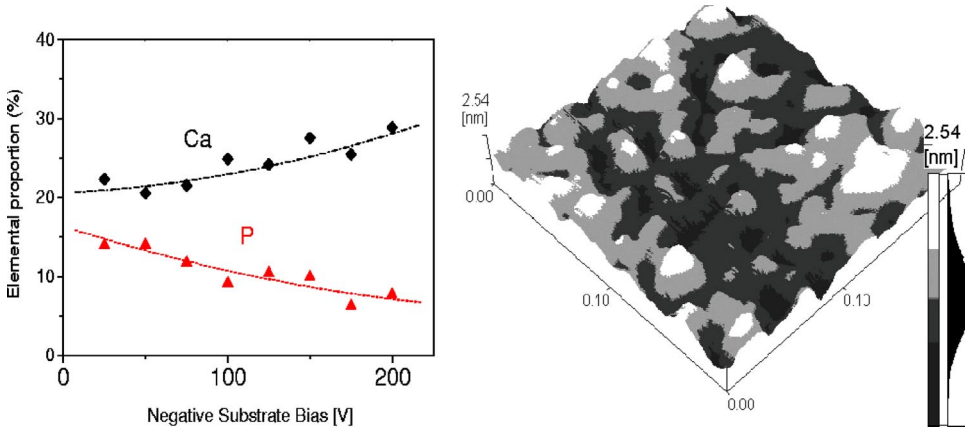

FIG. 13. (Color in online edition) Hydroxyapatite (HA) fabricated by reactive-plasma-assisted rf magnetron sputtering deposition: left, control of Ca and P content based on the different responses of cationic CaO^+ and anionic PO_4^{3-} building units to a negative substrate bias variation; right, representative AFM image of nanoscaled surface morphology (Xu, Long, *et al.*, 2005).

high resorption rates of the coating in the body's environment and, as a result, disastrous *in vivo* performance. Another drawback of this coating technique is the weak adhesive strength of the HA-metal implant interface, which often results in violent mechanical failures and significant implant degradation.

An alternative approach capitalizes on intentional disintegration of compressed commercial HA powder into smaller subnano (atomic, molecular) and nano- (macromolecular, nanocluster, and nanoparticle) building units in low-pressure reactive plasma environments (Long, Yu, Cai, *et al.*, 2002; Long, Xu, Lu, *et al.*, 2002b; Xu, Long, *et al.*, 2005). The reactive-plasma-assisted rf concurrent magnetron sputtering of HA and Ti targets is used as an ideal practical framework for the above bioceramic synthesis. More importantly, by using smaller building units and lower process temperatures, it appears possible to grow highly crystalline films and substantially improve the adhesive strength of the bioceramic-implant alloy interface. Transport of the main calcium- and phosphorus-bearing species (CaO^+ and PO_4^{3-}, respectively) to Ti-6Al-4V deposition substrates can be efficiently controlled by varying the dc bias. The different responses of oppositely charged CaO^+ and PO_4^{3-} species to the dc substrate bias make it possible to control absolute and relative elemental concentrations of calcium and phosphorus in the films, as shown in Fig. 13. Thus CaO^+ cations generated in Ar $+H_2O$ plasma discharges can be regarded as a cause of the elevated presence of calcium in the bioceramic, with a similar conclusion for the phosphorus-bearing anion PO_4^{3-}. In this set of experiments, there were no specific means of surface preparation for the deposition of the building units other than conventional pretreatment in argon and maintaining substrate temperatures high enough (usually in excess of 550 °C) to promote the required degree of crystallization. We emphasize that by using atomic, radical, and, presumably, nanocluster building units, one can obtain compact and dense films with a nanoscale surface morphology (Fig. 13) believed to be ideal to support biomolecule-bioceramic interactions resulting in enhanced bone ingrowth and remodeling. The hydroxyapatite films prepared by the rf magnetron concurrent sputtering technique feature excellent bioactivity and cytocompatibility, as suggested by *in vitro* simulated body fluid and osteoblast cell-culture assessments. Specific application of the four-stage cause and effect approach for reactive-plasma-assisted nanofabrication of HA bioceramics warrants substantial theoretical and experimental effort in the future.

There are many other examples of the excellent performance of reactive-plasma-based nanofabrication tools and techniques. One of the most recent examples is the plasma-assisted deposition of the superhard nanocomposite $nc\text{-}Al_xTi_{1-x}N/a\text{-}Si_3N_4$. This material is currently used in industrial tooling applications owing to its extra-high hardness, comparable to natural diamond; it significantly improves the lifetime of high-speed cutting bits (Veprek *et al.*, 2003). In a sense, this class of nanostructured materials is quite similar to the polymorphous silicon films considered in Sec. IV.A. Indeed, $Al_xTi_{1-x}N$ nanocrystals are embedded in the amorphous silicon nitride matrix. The highest hardness is achieved when each of the $Al_xTi_{1-x}N$ nanocrystals is covered by a monolayer of $a\text{-}Si_3N_4$ (Veprek *et al.*, 2004). It is a challenge for the future to invoke the "cause and effect" approach advocated here to learn more about the generation of nanocrystalline building units in the gas phase, surface activation, the transport of the building units towards the deposition substrates, and eventually, the deposition of the amorphous phase with rates just sufficient to coat the dynamically growing $Al_xTi_{1-x}N$ nanocrystals with an amorphous monolayer.

We emphasize that the continuum of nanofabrication processes, devices, materials, nanostructures, tools, and techniques in which reactive plasmas can be used is virtually infinite and, due to limited space, cannot be covered in a single Colloquium. Below we shall therefore briefly discuss only a few emerging applications and refer interested readers to more detailed references on this subject. Currently, reactive plasmas are widely used by the microelectronics industry for ultrafine selective

etching of submicron and nanofeatures (currently as small as ~130 nm, with an expected reduction to ~50 nm in the near future) of ultra-large-scale integrated circuits and devices (Lii, 1996; Oehrlein, 2003). Etching processes greatly benefit from the presence of a reactive plasma. In particular, sheath electric-field-driven reactive cations can perform highly anisotropic etching (in the direction normal to the surface), which is problematic in conventional chemical (wet) etching processes. It is interesting to mention that hydrogen etching of graphite can be used to synthesize diamond films and carbon nanotips (considered in Sec. IV.B), even without hydrocarbon gas feedstock (Yang *et al.*, 2005).

One of the most recent important advances has been in the use of prefabricated ordered nanostructure arrays for pattern transfers to solid surfaces. Examples include synthesis of Si nanopillar arrays in inductively coupled plasmas by using a lithographic mask made of nickel nanodots (Kim *et al.*, 2005) and nanofabrication of GaN-based nanorod light-emitting diodes using reactive ion etching in inductively coupled plasmas through self-assembled nickel nanomasks (Huang *et al.*, 2004).

A combination of ultrafine plasma etching with conventional lithographic techniques holds great promise for miniaturization of the features of integrated circuitry. Indeed, reactive oxygen plasma etching-enhanced nanolithography has been recently used for pattern transfer in nanofabrication of a 23-nm-period grating (believed to be the shortest-period grating defined by electron beam lithography) on diamond substrates (Lister *et al.*, 2004).

Nanopatterns can also be transferred onto solid substrates by utilizing reactive plasma etching through nanoporous templates. This approach has been noted in a recent report on a generic nonlithographic nanofabrication method for creating nanoporous patterns on any substrate by using nanoporous alumina as an etching mask (Menon *et al.*, 2004).

Another emerging area of nanofabrication is a precision treatment of porous materials with micron-sized and nanosized pore features (Cho, Rodriguez, *et al.*, 2005; Hua *et al.*, 2005), such as high-aspect-ratio trenches in silicon wafers, templated mesoporous materials (e.g., aluminophospates; Kimura, 2005), carbon-based molecular sieves for gas separation (Wang and Hong, 2005), microporous polymeric cytoscaffolds for bio-implants and tissue engineering, and several others.

A wide range of subnanosized building units in the plasma environment turns out to be favorable for the fabrication of complex nano-objects representing a variety of structural organizations and elemental compositions, which are quite difficult to synthesize by using other methods. There have been recent reports on the successful plasma-assisted synthesis of self-organized GaN quantum dot assemblies on ternary $Al_xGa_{1-x}N$ (Panin *et al.*, 2005); of periodic two-dimensionally arrayed nanocolumns made of the quarternary compound InGaAsP (Lee *et al.*, 2005); of various low-dimensional semiconductor structures, such as Ga_2O_3 and Al_2O_3 nanowires (Arnault and Devaux, 2004) and germanium quantum dots on silicon oxide (Shieh *et al.*, 2004), etc.

Structural incorporation of nanosized building units (considered in detail in Sec. IV.A) has recently been reported as an efficient solution in various nanofabrication processes. In particular, silicon nanocrystals or quantum dots can be embedded in a silicon nitride matrix to fabricate light-emitting diodes and other nanodevices (Cho, Park, *et al.*, 2005; Pei *et al.*, 2005).

The flexibility of the reactive plasma environment allows one to combine different nanostructures in the same device. Tetramethyl silane plasmas have been used for highly controllable, reactive-plasma-aided nanofabrication of nanocantilevers made of crystalline beta-SiC nanowires in silicon oxide nanocones (Lin *et al.*, 2004). Moreover, it has recently become possible to assemble new silicon-carbon heteronanostructures comprising multiwalled carbon nanotubes and tapered silicon nanowires (Song *et al.*, 2004). These unique nanostructures herald a new era of integration of carbon and silicon nanofeatures in nanoelectronic devices.

From a more traditional point of view, reactive plasmas remain a very efficient medium for synthesis and processing of advanced nanopowder and nanofilm materials. Very recent examples include manufacturing of polymer-coated silver nanopowder in microwave plasma chemical vapor deposition (Chau *et al.*, 2005) and sintering of nanocomposite Cu-TiB_2 powders (Kwon *et al.*, 2005). On the other hand, reactive plasmas of vinyltrymethylsilane and CO_2 gas mixtures have been successfully used for synthesis of nanocomposite low-k SiCOH films (Jeong *et al.*, 2004).

V. CONCLUSIONS AND OUTLOOK

The types of nanoassemblies, as well as of approaches to fabricating them, are increasing daily. While we have not been able to consider more than a fraction of the process-specific techniques, it is plain from those we have looked at that reactive plasmas have several important features that warrant their consideration as a versatile nanofabrication tool. By adopting the framework of the "cause and effect" approach, we have looked in turn at generation of the required building units in the ionized gas phase, the plasma-assisted preparation of and transport of the building units towards the deposition surfaces, and, finally, the stacking of the building units into the required nanoassembly patterns. The adopted framework has helped to elucidate many unique features of the selected nanofabrication methods and techniques.

There are numerous future challenges along the pathway to reactive-plasma-aided nanofabrication. For example, the accuracy of any process critically depends on the ability to detect and control the building units in the ionized gas phase. The existing experimental methods adequately monitor the building units at the smaller- and larger-size ends of the continuum but often fall short in the size range of small nanoclusters, which have recently been argued to be the most important building units for various nanoassemblies, thin films, and bulk

materials. Thus building units of this size range remain a challenge for the development of suitable *in situ* diagnostic techniques. Another challenge is to control the energetics of insertion of radical/molecular building units into nanoassemblies by the electric fields in the plasma sheath, and to optimize the discharge and process parameters.

Meanwhile, industrial applications of plasma-assisted deposition and control continue to expand. It is now evident that, by the use of charged nanoclusters or cation/anion radicals, one can deposit highly crystalline films at low substrate temperatures. This will enable thin-film industries to use cheaper polymer substrates (which are sensitive to high temperatures) and ultimately to improve cost efficiencies. On the other hand, aligned carbon nanotubes are promising for various nanoelectronic applications (Choi *et al.*, 2004). Owing to their small dimensions and unique metallic and semiconductor properties, carbon nanotubes have been suggested as an alternative material to be used when the physical limits of silicon-based microelectronics are reached (Collard *et al.*, 2005).

Looking beyond the applications of reactive plasmas at nanoscales, we note that plasma intrinsically is capable of producing a variety of atomic and ionic building units, and as such, holds great promise for the future processing of matter at atomic scales. A recent report on a high-precision, highly conformal plasma-aided technique of atomic layer deposition (Lee, 2005) sounds very encouraging.

We hope that this topic will attract the interest and critical comments of a wide interdisciplinary community and result in dedicated experiments to establish direct and conclusive correlations between the abundance of very specific building units in the ionized gas phase, the parameters of transition areas between the plasma bulk and substrates, the energetics of the building units upon deposition/stacking, and the key properties of the nanoassemblies. In the examples discussed above, the degree of such correlation varies, depending on the knowledge available to date.

In this Colloquium, one can also find a practical approach for the optimal choice of building unit and the plasma/process parameters to fabricate the desired nanoassembly. However, we have not aimed to provide exhaustive recipes for a reactive-plasma-assisted nanoassembly processes. The advocated "cause and effect" approach provides a conceptual framework not only for plasma-based nanofabrication, but also for the wider context of "nanobricklaying." We believe that reactive plasmas have a bright future for a wide range of applications as a versatile fabrication tool of the "nano age" and beyond.

ACKNOWLEDGMENTS

The author thanks M. Bilek, I. Denysenko, N. M. Hwang, I. Levchenko, V. Ligatchev, J. D. Long, D. R. McKenzie, P. A. Robinson, P. Roca i Cabarrocas, P. Rutkevych, L. Stenflo, R. Storer, H. Sugai, Z. Tsakadze, S. Veprek, S. V. Vladimirov, S. Xu, and M. Y. Yu, as well as many of his colleagues, for fruitful collaborations, discussions, and critical comments. He thanks also all authors of original figures for their kind permission to reproduce them. This work was partially supported by the Australian Research Council, the University of Sydney, and the Agency for Science, Technology, and Research (Singapore).

REFERENCES

American Society for Testing and Materials (ASTM), 2003, *Standard Specification for Composition of Hydroxyapatite for Surgical Implants* (ASTM, New York), F1185-03; see also http://www.astm.org

Arnault, C., and X. Devaux, 2004, J. Mater. Sci. Technol. **20**, 63.

Bapat, A., C. R. Perrey, S. A. Campbell, C. B. Carter, and U. Kortshagen, 2003, J. Appl. Phys. **94**, 1969.

Barnes, M. C., A. R. Gerson, S. Kumar, and N. M. Hwang, 2003, Thin Solid Films **436**, 181.

Barnes, M. C., A. R. Gerson, S. Kumar, and N. M. Hwang, 2004, Thin Solid Films **446**, 29.

Barnes, M. C., S. Kumar, L. Green, N. M. Hwang, and A. R. Gerson, 2005, Surf. Coat. Technol. **190**, 321.

Baron, T., P. Gentile, N. Magnea, and P. Mur, 2001, Appl. Phys. Lett. **79**, 1175.

Bethune, D. S., C. H. Kiang, M. S. DeVries, G. Gorman, R. Savoy, and R. Beyers, 1993, Nature (London) **363**, 605.

Bhandarkar, U. V., M. T. Swihart, S. L. Girshik, and U. Kortshagen, 2000, J. Phys. D **33**, 2731.

Boufendi, L., W. Stoffels, and E. Stoffels, 1999, in *Dusty Plasmas: Physics, Chemistry and Technological Impacts in Plasma Processing*, edited by A. Bouchoule (Wiley, New York), p. 181.

Bower, C., W. Zhu, S. Jin, and O. Zhou, 2000, Appl. Phys. Lett. **77**, 830.

Chaabane, N., A. V. Kharchenko, H. Vach, and P. Roca i Cabarrocas, 2003, New J. Phys. **3**, 37.1.

Chaabane, N., P. Roca i Cabarrocas, and H. Vach, 2004, J. Non-Cryst. Solids **338-340**, 51.

Chau, J. L. H., M. K. Hsu, C. C. Hsieh, and C. C. Kao, 2005, Mater. Lett. **59**, 905.

Chhowalla, M., K. B. K. Teo, C. Ducati, N. L. Rupersinghe, G. A. J. Amaratunga, A. C. Ferrari, D. Roy, J. Robertson, and W. I. Milne, 2001, J. Appl. Phys. **90**, 5308.

Cho, K. S., N. M. Park, T. Y. Kim, K. H. Kim, G. Y. Sung, and J. H. Shin, 2005, Appl. Phys. Lett. **86**, 071909.

Cho, W. J., O. Rodriguez, R. Saxena, M. Ojha, R. A. Chanta, J. L. Plawsky, and W. N. Gill, 2005, J. Electrochem. Soc. **152**, F26.

Choi, W. B., E. Bae, D. Kang, S. Chae, B. Cheong, J. Ko, E. Lee, and W. Park, 2004, Nanotechnology **15**, S512.

Collard, C., J. P. Holloway, and M. L. Brake, 2005, IEEE Trans. Plasma Sci. **33**, 170.

Costa, J., 2000, in *Handbook of Nanostructured Materials*, edited by H. S. Nalva (Academic, New York), Vol. 1, p. 57.

De Bleecker, K., A. Bogaerts, R. Gijbels, and W. Goedheer, 2004, Phys. Rev. E **69**, 056409.

Denysenko, I. B., K. Ostrikov, S. Xu, M. Y. Yu, and C. H. Diong 2003, J. Appl. Phys. **94**, 6097.

Denysenko, I. B., S. Xu, P. P. Rutkevych, J. D. Long, N. A.

Azarenkov, and K. Ostrikov, 2004, J. Appl. Phys. **95**, 2713.
Dresselhaus, M. S., G. Dresselhaus, and P. C. Eklund, 1996, *Science of Fullerenes and Carbon Nanotubes* (Academic, New York).
Fontcuberta i Morral, A., and P. Roca i Cabarrocas, 2001, Thin Solid Films **383**, 161.
Fontcuberta i Morral, A., P. Roca i Cabarrocas, and C. Clerc, 2004, Phys. Rev. B **69**, 125307.
Franklin, N. R., and H. Dai, 2002, Adv. Mater. (Weinheim, Ger.) **12**, 890.
Frantz, J., and K. Nordlund, 2003, Phys. Rev. B **67**, 075415.
Frenklash, M., and H. Wang, 1991, Phys. Rev. B **43**, 1520.
Fridman, A., and L. A. Kennedy, 2004, *Plasma Physics and Engineering* (Taylor & Francis, New York).
Fridman, A. A., L. Boufendi, T. Hbid, B. N. Potapkin, and A. Bouchoule, 1996, J. Appl. Phys. **79**, 1303.
Gebauer, G., and J. Winter, 2003, New J. Phys. **5**, 38.1.
Gerhardt, P., and K. H. Homann, 1990, Combust. Flame **81**, 289.
Ghidini, R., C. H. J. M. Groothuis, M. Sorokin, G. M. W. Kroesen, and W. W. Stoffels, 2004, Plasma Sources Sci. Technol. **13**, 143.
Gilbert, B., F. Huang, H. Zhang, G. Waychunas, and J. F. Banfield, 2004, Science **305**, 651.
Gordillo-Vazques, F. J., and J. M. Albella, 2004, Plasma Sources Sci. Technol. **13**, 50.
Goree, J., and T. E. Sheridan, 1992, J. Vac. Sci. Technol. A **10**, 3540.
Gruen, D. M., 2001, MRS Bull. **26**, 771.
Gruen, D. M., P. C. Redfern, D. A. Horner, P. Zapol, and L. A. Curtis, 1999, J. Phys. Chem. B **103**, 5459.
Hash, D., and M. Meyyappan, 2003, J. Appl. Phys. **93**, 750.
Helveg, S., C. Lopez-Cartez, J. Sehested, P. L. Hansen, B. S. Clausen, J. R. Rostrup-Nielsen, F. Abild-Pedersen, and J. Norskov, 2004, Nature (London) **427**, 426.
Hirata, T., N. Satake, G. H. Jeong, and T. Kato, 2003, Appl. Phys. Lett. **83**, 1119.
Hofmann, S., C. Dukati, J. Robertson, and B. Kleinsorge, 2003, Appl. Phys. Lett. **83**, 135.
Hollenstein, C., 2000, Plasma Phys. Controlled Fusion **42**, R93.
Hong, S., J. Berndt, and J. Winter, 2003, Plasma Sources Sci. Technol. **12**, 46.
Hrivnak, B. J., and S. Kwok, 1999, Astrophys. J. **513**, 869.
Hua, X. F., C. Stolz, G. S. Oehrlein, P. Lazzeri, N. Coghe, M. Anderle, C. K. Inoki, M. Anderle, T. S. Kuan, and P. Jiang, 2005, J. Vac. Sci. Technol. A **23**, 151.
Huang, H. W., C. C. Kao, T. H. Hsueh, C. C. Yu, C. F. Lin, J. T. Chu, H. C. Kuo, and S. C. Wang, 2004, Mater. Sci. Eng., B **113**, 125.
Hwang, N. M., 1999, J. Cryst. Growth **204**, 85.
Hwang, N. M., W. S. Cheong, D. Y. Yoon, and D. Y. Kim, 2000, J. Cryst. Growth **218**, 33.
Hwang, N. M., J. H. Hahn, and D. Y. Yoon, 1996, J. Cryst. Growth **162**, 55.
Hwang, N. M., and D. Y. Kim, 2004, Int. Mater. Rev. **49**, 171.
Hwang, N. M., and D. Y. Yoon, 1994, J. Cryst. Growth **143**, 103.
Iijima, S., 1991, Nature (London) **354**, 56.
Jeon, I. D., C. J. Park, D. Y. Kim, and N. N. Hwang, 2000, J. Cryst. Growth **213**, 79.
Jeong, K. H., S. G. Park, and S. W. Rhee, 2004, J. Vac. Sci. Technol. B **22**, 2799.
Kanzow, H., and A. Ding, 1999, Phys. Rev. B **60**, 11180.
Kersten, H., R. Wiese, G. Thieme, M. Froehlich, A. Kopitov, D. Bojic, F. Scholze, H. Neumann, M. Quaas, H. Wulff, and R. Hippler, 2003, New J. Phys. **5**, 93.1.
Kim, M. J., J. S. Lee, S. K. Kim, G. Y. Yeom, J. B. Yoo, and C. Y. Park, 2005, Thin Solid Films **475**, 41.
Kimura, T., 2005, Microporous Mesoporous Mater. **77**, 97.
Klein, C. P. A. T., P. Patsa, J. G. C. Wolke, J. Blieck-Hogervorst, and K. Groot, 1994, J. Biomed. Mater. Res. **28**, 909.
Kovacevic, E., I. Stefanovic, J. Berndt, and J. Winter, 2003, J. Appl. Phys. **93**, 2924.
Kuykendall, T., P. J. Pauzauskie, Y. Zhang, J. Goldberger, D. Sirbuly, J. Denlinger, and P. Yang, 2004, Nat. Mater. **3**, 524.
Kwon, Y. S., J. S. Kim, P. P. Choi, J. H. Song, and D. Dudina, 2005, J. Ind. Eng. Chem. (Seoul, Repub. Korea) **11**, 103.
Lee, J. M., S. H. Oh, C. W. Lee, H. Ko, S. Park, K. S. Kim, and M. H. Park, 2005, Thin Solid Films **475**, 189.
Lee, Y. J., 2005, Mater. Lett. **59**, 615.
Levchenko, I., M. Korobov, M. Romanov, and M. Keidar, 2004, J. Phys. D **37**, 1690.
Levchenko, I., and K. Ostrikov, 2005, unpublished.
Lieberman, M. A., and A. J. Lichtenberg, 1994, *Principles of Plasma Discharges and Materials Processing* (Wiley, New York).
Lii, Y. J. T., 1996, in *ULSI Technology*, edited by C. Y. Chang and S. M. Sze (McGraw-Hill, New York), p. 329.
Lin, M., K. P. Loh, C. Boothroyd, and A. Y. Du, 2004, Appl. Phys. Lett. **85**, 5388.
Lister, K. A., B. G. Casey, P. S. Dobson, S. Thoms, D. S. Macintyre, C. D. W. Wilkinson, and J. M. R. Weaver, 2004, Microelectron. Eng. **73-74**, 319.
Long, J. D., P. P. Rutkevych, J. Z. Wu, and S. Xu, 2005, unpublished.
Long, J. D., S. Xu, J. W. Cai, N. Jiang, J. H. Lu, K. N. Ostrikov, and C. H. Diong, 2002, Mater. Sci. Eng., C **20**, 175.
Long, J. D., S. Xu, J. H. Lu, K. N. Ostrikov, and C. H. Diong, 2002, IEEE Trans. Plasma Sci. **30**, 118.
Louchev, O. A., and J. R. Hester, 2003, J. Appl. Phys. **94**, 2002.
Magnano, E., C. Cepek, M. Sancrotti, F. Siviero, S. Vinati, C. Lenardi, P. Piseri, E. Barborini, and P. Milani, 2003, Phys. Rev. B **67**, 125414.
Marks, N., J. M. Bell, G. K. Pearce, D. R. McKenzie, and M. M. M. Bilek, 2003, Diamond Relat. Mater. **12**, 2003.
Marks, N., N. C. Cooper, D. R. McKenzie, D. G. McCulloch, P. Bath, and S. P. Russo, 2002, Phys. Rev. B **65**, 075411.
Menon, L., K. B. Ram, S. Patibandla, D. Aurongzeb, M. Holtz, J. Yun, V. Kuryatkov, and K. Zhu, 2004, J. Electrochem. Soc. **151**, C492.
Merkulov, V. I., A. V. Melechko, M. A. Guillorn, D. H. Lowndes, and M. L. Simpson, 2000, Appl. Phys. Lett. **76**, 3555.
Merkulov, V. I., A. V. Melechko, M. A. Guillorn, D. H. Lowndes, and M. L. Simpson, 2001, Appl. Phys. Lett. **79**, 2970.
Merlino, R., and J., Goree, 2004, Phys. Today **57** (7), 32.
Meyyappan, M., L. Delzeit, A. Cassel, and D. Hash, 2003, Plasma Sources Sci. Technol. **12**, 205.
Monticone, S., R. Tufeu, A. V. Kanaev, E. Scolan, C. Sanchez, 2000, Appl. Surf. Sci. **162**, 565.
Mulvaney, P., 2001, MRS Bull. **26**, 1009.
Obraztsov, A. N., I. Pavlovsky, A. P. Volkov, E. D. Obraztsova, A. L. Chuvilin, and V. L. Kuznetsov, 2000, J. Vac. Sci. Technol. B **18**, 1059.

Oehrlein, G. S., 2003, *Plasma Processing of Electronic Materials* (Springer, Berlin).
Ostraat, M. L., J. W. De Blauwe, M. L. Green, L. D. Bell, M. L. Brongersma, J. Casperson, R. C. Flagan, and H. A. Atwater, 2001, Appl. Phys. Lett. **79**, 433.
Ostrikov, K., I. B. Denysenko, S. V. Vladimirov, S. Xu, H. Sugai, and M. Y. Yu, 2003, Phys. Rev. E **67**, 056408.
Ostrikov, K., I. Denysenko, M. Y. Yu, C. H. Diong, and S. Xu, 2005, Phys. Scr. (to be published).
Panin, G. N., Y. S. Park, T. W. Kang, T. W. Kim, K. L. Wang, and M. Bao, 2005, J. Appl. Phys. **97**, 043527.
Pei, Z. W., A. Y. K. Su, H. L. Hwang, and H. L. Hsiao, 2005, Appl. Phys. Lett. **86**, 063503.
Perrin, J., and C. Hollenstein, 1999, in *Dusty Plasmas: Physics, Chemistry and Technological Impacts in Plasma Processing*, edited by A. Bouchoule (Wiley, New York), p. 77.
Perrin, J., M. Shiratani, P. Kae-Nune, H. Videlot, J. Jolly, and J. Guillon, 1998, J. Vac. Sci. Technol. A **16**, 278.
Pitkethly, M. J., 2003, Nano Today, 36.
Poissant, Y., P. Chatterjee, and P. Roca i Cabarrocas, 2003, J. Appl. Phys. **94**, 7305.
Poole, C. P., Jr., and F. J. Owens, 2003, *Introduction to Nanotechnology* (Wiley, New York).
Roca i Cabarrocas, P., N. Chaabane, A. V. Kharchenko, and S. Tchakarov, 2004, Plasma Phys. Controlled Fusion **46**, B235.
Roca i Cabarrocas, P., S. Hamma, S. N. Sharma, G. Viera, E. Bertran, and J. Costa, 1998, J. Non-Cryst. Solids **227-230**, 871.
Roco, M. C., S. Williams, and P. Alivisatos, 1999, *Nanotechnology Research Directions: Vision for Nanotechnology Research and Development in the Next Decade* (Kluwer Academic, Amsterdam); see also US National Nanotechnology Initiative, http://www.nano.gov
Rode, A. V., E. G. Gamaly, A. G. Christy, J. C. F. Gerald, S. T. Hyde, R. G. Elliman, B. Luther-Davies, A. I. Veinger, J. Androulakis, and J. Giapintzakis, 2004, Phys. Rev. B **70**, 054407.
Rutkevych, P. P., K. Ostrikov, S. Xu, and S. V. Vladimirov, 2004, J. Appl. Phys. **96**, 4421.
Shchukin, V., N. N. Ledentsov, and D., Bimberg, 2003, *Epitaxy of Nanostructures* (Springer, Berlin/Heidelberg).
Shieh, J., T. S. Ko, H. L. Chen, B. T. Dai, and T. C. Chu, 2004, Chem. Vap. Deposition **10**, 265.
Shiratani, M., K. Koga, and Y. Watanabe, 2003, Thin Solid Films **427**, 1.
Shiratani, M., S. Maeda, K. Koga, and Y. Watanabe, 2000, Jpn. J. Appl. Phys., Part 1 **39**, 287.
Song, S. P., M. A. Crimp, V. M. Ayres, C. J. Collard, J. P. Holloway, and M. L. Brake, 2004, J. Nanosci. Nanotechnol. **4**, 817.
Stangl, J., V. Holy, and G. Bauer, 2004, Rev. Mod. Phys. **76**, 725.
Stoffels, W. W., E. Stoffels, G. H. P. M. Swinkels, H. Videlot, M. Boufnichkel, and G. M. W. Kroesen, 1999, Phys. Rev. E **59**, 2302.
Stoykov, S., C. Eggs, and U. Kortshagen, 2001, J. Phys. D **34**, 2160.
Suendo, V., A. Kharchenko, and P. Roca i Cabarrocas, 2004, Thin Solid Films **451-452**, 259.
Sugai, H., I. Ghanashev, M. Hosokawa, K. Mizuno, K. Nakamura, H. Toyoda, and K. Yamauchi, 2001, Plasma Sources Sci. Technol. **10**, 378.
Suh, S. M., S. L. Girshik, U. R. Kortshagen, and M. R. Zachariah, 2003, J. Vac. Sci. Technol. A **21**, 251.
Sun, L., C. C. Berndt, K. A. Gross, and A. Kucuk, 2001, J. Biomed. Mater. Res. **58**, 570.
Tanda, M., M. Kondo, and A. Matsuda, 2003, Thin Solid Films **427**, 33.
Thomas, H. M., and G. E. Morphill, 1996, Nature (London) **379**, 806.
Tsai, S. H., F. K. Chiang, T. G. Tsai, F. S. Shieu, and H. C. Shih, 2000, Thin Solid Films **366**, 11.
Tsakadze, Z. L., K. Ostrikov, J. D. Long, and S. Xu, 2004, Diamond Relat. Mater. **13**, 1923.
Tsakadze, Z. L., K. Ostrikov, and S. Xu, 2005, Surf. Coat. Technol. **191/1**, 49.
Tsubouchi, K., and K., Masu, 1992, J. Vac. Sci. Technol. A **10**, 856.
Tsui, Y. C., C. Doyle, and T. W. Clyne, 1998, Biomaterials **19**, 2031.
Veprek, S., H.-D. Mannling, M. Jilek, and P. Holubar, 2004, Mater. Sci. Eng., A **366**, 202.
Veprek, S., S. Mukherjee, P. Karvankova, H.-D. Mannling, J. L. He, K. Moto, J. Prochazka, and A. S. Argon, 2003, J. Vac. Sci. Technol. A **21**, 532.
Viera, G., M. Mikikian, E. Bertran, P. Roca i Cabarrocas, and L. Boufendi, 2002, J. Appl. Phys. **92**, 4684.
Vladimirov, S. V., and K. Ostrikov, 2004, Phys. Rep. **393**, 175.
Walch, S., and R. Merkle, 1998, Nanotechnology **9**, 1998.
Wang, L. J., and F. C. N. Hong, 2005, Microporous Mesoporous Mater. **77**, 167.
Xu, S., J. D. Long, L. Sim, C. H. Diong, and K. Ostrikov, 2005, Plasma Proc. Polym. **2**, 373.
Xu, S., K. Ostrikov, J. D. Long, and S. Y. Huang, 2005, unpublished.
Yang, Q., W. Chen, C. Xiao, R. Sammynaiken, and A. Hirose, 2005, Carbon **43**, 748.
Yasuda, H., 1985, *Plasma Polymerization* (Academic, New York).